

A search for HI 21cm absorption in strong MgII absorbers in the redshift desert

N. Kanekar^{1*}, J. X. Prochaska², S. L. Ellison³, J. N. Chengalur⁴

¹*National Radio Astronomy Observatory, 1003 Lopezville Rd, Socorro, NM 87801, USA;*

²*UCO/Lick Observatory, UC Santa Cruz, Santa Cruz, CA 95064, USA;*

³*Department of Physics and Astronomy, University of Victoria, Victoria, B.C., V8P 1A1, Canada*

⁴*National Centre for Radio Astrophysics, Ganeshkhind, Pune 411007, India*

Received mmdyy/ accepted mmdyy

ABSTRACT

We report results from a deep search for redshifted HI 21cm absorption in 55 strong MgII λ 2796 absorbers (having $W_0^{\lambda 2796} > 0.5\text{\AA}$) at intermediate redshifts, $0.58 < z_{\text{abs}} < 1.70$, with the Green Bank Telescope (GBT) and the Giant Metrewave Radio Telescope (GMRT). Nine detections of HI 21cm absorption were obtained, all at $1.17 < z_{\text{abs}} < 1.68$, including three systems reported earlier by Gupta et al. (2007). Absorption was not detected at $> 3\sigma$ significance in 32 other MgII absorbers, with 26 of these providing strong upper limits to the HI 21cm optical depth, $\tau_{3\sigma} < 0.013$ per $\sim 10 \text{ km s}^{-1}$. For the latter 26 systems, the spin temperature T_s of the absorber must be $> [800 \times f] \text{ K}$ (where f is the covering factor), if the HI column density is $\geq 2 \times 10^{20} \text{ cm}^{-2}$, i.e. if the absorber is a damped Lyman- α system (DLA). Data on the remaining 13 systems of the sample were affected by radio frequency interference and were hence not useful.

Two of the MgII absorbers, at $z_{\text{abs}} \sim 1.4106$ towards 2003–025 and at $z_{\text{abs}} \sim 0.9115$ towards 2149+212, are known DLAs. We detect HI 21cm absorption towards 2003–025 with the GMRT and estimate the spin temperature of the DLA to be $T_s = [(905 \pm 380) \times f] \text{ K}$. Conversely, the GBT observations of 2149+212 resulted in a non-detection of HI 21cm absorption, yielding the 3σ limit $T_s > [2700 \times f] \text{ K}$.

Excluding “associated” systems (within 3000 km s^{-1} of the quasar redshift), the detection rate of HI 21cm absorption in strong MgII λ 2796 absorbers is $x_{21, \text{MgII}}(\bar{z} = 1.1) = 25_{-8}^{+11}\%$, at a 3σ optical depth sensitivity of ~ 0.013 per 10 km s^{-1} . Comparing the detection rates of HI 21cm and damped Lyman- α absorption in strong MgII absorber samples yields a detection rate of HI 21cm absorption in DLAs of $x_{21, \text{DLA}}(\bar{z} = 1.1) = (73 \pm 27)\%$, consistent with the detection rate in low- z DLAs. Since HI 21cm absorption arises in cold neutral gas, this indicates that most gas-rich galaxies contain significant fractions of cold HI by $z \sim 1$.

Finally, we use the observed detection rate of HI 21cm absorption in MgII absorbers to infer the cosmological mass density of neutral gas in DLAs, assuming that (1) the average HI column density in our HI 21cm absorber sample is the same as that measured by Rao et al. (2006) in their DLA sample, and (2) the detection rate of HI 21cm absorption in the DLAs of our MgII sample is the same as that in known DLAs at $0.09 < z_{\text{abs}} < 3.45$. We obtain $\Omega_{\text{GAS}} \sim (0.55_{-0.22}^{+0.42}) \times 10^{-3}$, at $\bar{z} \sim 1.1$, slightly lower than, but consistent with, the value obtained by Rao et al. (2006) from their DLA survey at similar redshifts.

Key words: galaxies: evolution: – galaxies: ISM – radio lines: galaxies

1 INTRODUCTION

Much of what is known about gas-rich galaxies at high redshifts comes from studies of the highest HI column density systems de-

tected in the spectra of distant quasars, the damped Lyman- α absorbers [DLAs, with $N_{\text{HI}} \geq 2.0 \times 10^{20} \text{ cm}^{-2}$; see, e.g., Wolfe et al. (2005) for a recent review]. Unlike objects such as Lyman-break or sub-mm galaxies obtained from emission (i.e. flux-limited) surveys, DLA samples are selected from absorption surveys and are hence not biased towards the high luminosity end of the galaxy distribution. Studies of DLAs over a range of redshifts thus provide

* E-mail: nkanekar@ao.nrao.edu (NK); xavier@ucolick.org (JXP); sarae@uvic.ca (SLE); chengalu@ncra.tifr.res.in (JNC)

direct observational constraints on the evolution of the predecessors of today's galaxies, and the gas therein.

Current DLA samples are strongly biased towards high redshifts ($z_{\text{abs}} > 1.7$, for which the Lyman- α line redshifts into optical wavebands), as it has not been possible to carry out large blind DLA surveys with space-based facilities. There are only ~ 50 known DLAs at $z_{\text{abs}} < 1.7$ (e.g. Rao et al. 2006; hereafter RTN06), while more than a thousand have been found at $z_{\text{abs}} \gtrsim 2$, primarily from searches based on the Sloan Digital Sky Survey (SDSS; Prochaska & Herbert-Fort 2004; Prochaska et al. 2005¹). Optical imaging studies have found low redshift DLAs to be associated with a mixture of galaxy types, including dwarfs, low surface brightness systems and luminous spiral disks (e.g. le Brun et al. 1997; Rao et al. 2003; Chen & Lanzetta 2003). However, at high redshifts, $z \gtrsim 1$, their small angular separation from the much brighter background quasars has meant that it is very difficult to directly image the absorbing galaxies. As a result, detailed studies of high- z DLAs have mostly been limited to high-resolution absorption spectroscopy. While such studies have provided much information on physical conditions in the absorbers, they have also given rise to some conundrums, partly, no doubt, due to the mix of morphologies, impact parameters and orientations in the high- z DLA population. For example, while DLA metallicities, measured in ~ 150 absorbers (including ~ 25 at $z_{\text{abs}} < 1.7$; Akerman et al. 2005; Meiring et al. 2006; Prochaska et al. 2007), do show evidence for an increase with decreasing redshift (Kulkarni & Fall 2002; Prochaska et al. 2003; Kulkarni et al. 2005), low metallicities (one-tenth solar or lower) are the norm at all redshifts (e.g. Pettini et al. 1999; Kulkarni et al. 2005; Prochaska et al. 2007). Contrary to expectations from most models of chemical evolution (e.g. Pei et al. 1999), the extrapolated mean DLA metallicity at $z = 0$ is well below solar values (although see Zwaan et al. 2005). Similarly, while it has been argued that typical abundance patterns in DLAs indicate star formation histories similar to those of dwarf galaxies (e.g. Dessauges-Zavadsky et al. 2007), it is difficult to explain the large observed velocity widths ($\gtrsim 100 \text{ km s}^{-1}$) by absorption in individual dwarfs (Prochaska & Wolfe 1997). These and other problems have meant that, despite more than two decades of systematic study, the nature of, and physical conditions in, high z DLAs, as well as their redshift evolution, remain issues of much controversy.

For DLAs lying towards radio-loud background quasars, absorption studies in the redshifted H I 21cm line can be used to derive additional information on physical conditions in the absorber [see Kanekar & Briggs (2004) for a review]. Combining the H I column density of the DLA (determined from the Lyman- α line) and the integrated H I 21cm optical depth yields the column-density-weighted harmonic mean spin temperature T_s of the neutral hydrogen, which gives the distribution of the gas between the warm and cold phases. The spin temperature is one of the few direct probes of physical conditions in the neutral gas in DLAs; most optical techniques infer conditions in the H I from observations of the low-ionization metal lines, which are assumed to be associated with the neutral hydrogen (e.g. Wolfe et al. 2005). Further, most optical resonance transitions (including Lyman- α) are quite insensitive to physical conditions like density and temperature.

Low- z DLAs show a mix of low and high spin temperatures (see Fig. 3 of Kanekar & Chengalur 2003), while DLAs at $z_{\text{abs}} \gtrsim 1.7$ typically have high spin temperatures, $T_s \gtrsim$

1000 K (e.g. Carilli et al. 1996; Chengalur & Kanekar 2000; Kanekar & Chengalur 2003). So far, only one DLA at $z_{\text{abs}} \gtrsim 1.7$ has been found to have $T_s < 500 \text{ K}$ (York et al. 2007). Further, the fraction of detections of H I 21cm absorption is significantly higher at $z_{\text{abs}} < 0.7$ ($\sim 85\%$) than at $z_{\text{abs}} > 1.7$ [$\sim 33\%$; Kanekar et al. (*in prep.*)]. Note that searches for H I 21cm absorption in DLAs are usually carried out to a sensitivity limit in spin temperature (usually $\gtrsim 800 \text{ K}$; e.g. Kanekar & Chengalur 2003), thus taking into consideration the H I column density of the DLA, rather than to a fixed H I 21cm optical depth sensitivity.

The redshift dependence of the spin temperature suggests an evolution in the temperature distribution of the DLAs, due to either evolving physical conditions within the DLA galaxies or changes in the nature of the galaxies that typically give rise to DLAs at a given redshift. In the local Universe, large spiral galaxies (including the Milky Way) tend to have low spin temperatures ($T_s \lesssim 300 \text{ K}$; e.g. Braun & Walterbos 1992), indicating large cold gas fractions. On the other hand, warm gas has been found to dominate the temperature distribution in dwarfs (e.g. Young & Lo 1997). A similar trend between spin temperature and galaxy type has been seen in low- z DLAs, wherein absorbers associated with luminous disk galaxies have $T_s \lesssim 300 \text{ K}$, while absorbers associated with low luminosity galaxies have $T_s \gtrsim 800 \text{ K}$ (Chengalur & Kanekar 2000). These results are suggestive of a scenario in which high- z DLAs are typically smaller systems like dwarfs, while low- z DLAs arise in both low and high luminosity galaxies (Kanekar & Chengalur 2001).

The spin temperature of DLAs thus appears to be one of the few tracers of physical conditions in DLAs that shows evidence for evolution with redshift and has hence been a subject of much interest and controversy (e.g. Kanekar & Chengalur 2003; Wolfe et al. 2003; Curran et al. 2005). A detailed understanding of the evolution of the spin temperature in DLAs has been hampered by the paucity of DLAs detected towards radio-loud quasars that are suitable for H I 21cm absorption studies. The situation has now improved at high redshifts, $z_{\text{abs}} \gtrsim 2$, primarily due to recent surveys for DLAs towards samples of quasars selected on the basis of their radio flux density (Ellison et al. 2001; Jorgenson et al. 2006; Ellison et al. 2008). However, there is yet a critical shortage of T_s measurements in the “redshift desert”, $0.7 < z_{\text{abs}} < 1.7$, as almost no DLAs have been found here towards radio-loud quasars. In fact, prior to this work, there was not a single spin temperature estimate in a “classical” DLA (i.e. with $N_{\text{HI}} \geq 2 \times 10^{20} \text{ cm}^{-2}$) in the redshift range $0.9 < z_{\text{abs}} < 1.7$, which encompasses more than a quarter of the history of the Universe. Unfortunately, it is precisely at these redshifts that the star formation activity in the Universe shows strong evolution, either peaking here or flattening, and then decreasing significantly to lower redshifts (e.g. Madau et al. 1996; Hopkins 2004). This redshift range is also likely to see significant evolutionary effects in the neutral gas, such as the build-up of the cold phase of H I and hence, the onset of stronger H I 21cm absorption and the transition to the high detection fraction and the low spin temperatures seen at low redshifts.

Besides probing physical conditions in the absorbing galaxies, detections of H I 21cm absorption are also important as a means of probing evolution in the fundamental constants [see Kanekar (2008) for a recent review]. A comparison between the absorption redshifts in the H I 21cm and optical resonance transitions allows a probe of changes in three fundamental constants, the fine structure constant α , the proton-electron mass ratio $\mu \equiv m_p/m_e$ and the proton g-factor g_p (Wolfe et al. 1976). Given that the H I 21cm and optical lines need not arise in the same gas, statistically large absorption samples must be used for the comparison, to ensure that

¹ <http://www.ucolick.org/~xavier/SDSSDLA/index.html>

any observed redshift offsets are not dominated by local systematic effects. The redshift desert $0.7 < z_{\text{abs}} < 1.7$ is the obvious place to attempt to set up a large sample of H I 21cm absorbers, if the fraction of cool gas increases significantly here. Note that the look-back time at $z \sim 1.7$ is ~ 9.8 Gyrs, implying that the comparison between H I 21cm and optical redshifts out to this redshift would probe $\sim 70\%$ of the age of the Universe.

The weakness of the H I 21cm transition, combined with observational issues such as radio frequency interference (RFI) at low frequencies, makes it very difficult to directly carry out a blind survey for H I 21cm absorption with current radio telescopes (e.g. Kanekar & Briggs 2004). In addition, almost no DLAs are known at $0.7 < z_{\text{abs}} < 1.7$ towards radio-loud quasars and it would be difficult to carry out space-based surveys for such DLAs. However, RTN06 found that systems with MgII λ 2796 and FeII λ 2600 rest equivalent widths larger than 0.5\AA have a $\sim (36 \pm 6)\%$ probability of being DLAs (see also Rao & Turnshek 2000). These transitions are detectable with ground-based optical telescopes at $z_{\text{abs}} \gtrsim 0.15$, implying that it should be possible to set up new samples of H I 21cm absorbers by targeting such “strong MgII absorbers” towards radio-loud quasars. Large samples of such MgII absorbers ($\sim 10^4$ systems) have been found in the SDSS, at $z_{\text{abs}} \gtrsim 0.4$ (e.g. Prochter et al. 2006), while the Complete Optical and Radio Absorption Line Systems (CORALS) survey (Ellison et al. 2004) obtained a smaller sample of such absorbers, but towards a radio-loud quasar sample, well-suited for follow-up H I 21cm absorption studies. We have used the Giant Metrewave Radio Telescope (GMRT) and the Green Bank Telescope (GBT) to carry out a deep search for redshifted H I 21cm absorption from a large sample of strong MgII absorbers in the redshift desert, selected from the above surveys. A similar program, carried out in parallel with ours on the GMRT, has recently detected three new H I 21cm absorbers at these redshifts (Gupta et al. 2007). The first results of our survey, based on GMRT and GBT observations of 55 absorbers, are presented in this paper.

2 THE MgII ABSORBER SAMPLE

We used MgII absorber samples drawn from the CORALS survey (Ellison et al. 2004), Data Releases (DRs) 3-5 of the SDSS (e.g. Prochter et al. 2006) and the literature (e.g. Sargent et al. 1988; Barthel et al. 1990; Aldcroft et al. 1994) to select our targets. The primary selection criterion was that the system be a “strong” MgII absorber, with $W_0^{\lambda 2796} \geq 0.5\text{\AA}$ (where $W_0^{\lambda 2796}$ is the MgII λ 2796 rest equivalent width), lying towards a background quasar of “sufficient” radio flux density at the redshifted H I 21cm line frequency to allow a sensitive search for H I 21cm absorption. A secondary criterion, that the rest equivalent width in the FeII λ 2600 transition also be large, $W_0^{\lambda 2600} \geq 0.5\text{\AA}$, was also typically used, although a few systems with $W_0^{\lambda 2600} < 0.5\text{\AA}$ or without information on $W_0^{\lambda 2600}$ were also observed. We thus have two effective sub-samples:

- (1) Systems with $W_0^{\lambda 2796} \geq 0.5\text{\AA}$ and $W_0^{\lambda 2600} \geq 0.5\text{\AA}$.
- (2) Systems with $W_0^{\lambda 2796} \geq 0.5\text{\AA}$ and either $W_0^{\lambda 2600} < 0.5\text{\AA}$ or no information on the $W_0^{\lambda 2600}$ transition.

The best optical depth sensitivities achieved in present searches for H I 21cm absorption in DLAs are $\tau_{3\sigma} \sim 0.01$ per $\sim 10 \text{ km s}^{-1}$ (e.g. Kanekar et al. 2006; York et al. 2007). For DLAs, with $N_{\text{HI}} \geq 2 \times 10^{20} \text{ cm}^{-2}$, a non-detection at this sensitivity would yield the 3σ limit $[T_s/f] \geq 1000 \text{ K}$. In other words, only

QSO	z_{em}	R mag	z_{abs}	$W_0^{\lambda 2796}$ \AA	$W_0^{\lambda 2600}$ \AA	$W_0^{\lambda 2852}$ \AA
0017+154	2.009	17.7 [†]	1.6260 ^a	1.44	0.76	0.48
0039–407	2.478	19.7 [†]	0.8483 ^b	2.35	2.09	–
0014+813	3.366	16.5	1.1109 ^c	0.85	0.53	0.20
0014+813	3.366	16.5	1.1125 ^c	2.49	2.14	0.40
0105–008	1.374	17.7	1.3710 ^a	0.58	0.38	0.22
0109+176	2.157	18.0	0.8392 ^d	1.75	1.09	< 0.2
0237–233	2.223	16.6	1.3647 ^e	2.05	0.84	< 0.16
0237–233	2.223	16.6	1.6724 ^j	1.31	0.57	0.47
0240–060	1.805	18.7 [†]	0.5810 ^b	1.44	–	0.11
0240–060	1.805	18.7 [†]	0.7550 ^b	1.65	1.25	0.63
0244–128	2.201	18.4 [†]	0.8282 ^b	1.77	1.23	0.45
0311+430	2.870	21.5 [†]	1.068 ^k	3.12	2.31	–
0409–045	1.684	19.9	0.8797 ^a	1.81	1.29	< 0.25
0445+097	2.108	19.6	0.8392 ^d	3.17	1.97	0.91
0458–020	2.286	19.0 [†]	1.5605 ^b	0.94	0.75	< 0.21
0642+449	3.396	18.5 [*]	1.2468 ^f	0.57	0.50	–
0741+294	1.184	17.1	1.0625 ^a	1.19	0.73	0.46
0801+303	1.451	18.3	1.1908 ^a	1.45	0.97	0.30
0804+499	1.436	19.0	1.4071 ^a	1.29	0.70	0.26
0812+332	2.426	19.4	0.8518 ^a	2.36	0.98	0.60
0821+394	1.216	18.5	1.0545 ^a	1.56	0.88	0.17
0829+425	1.051	18.9	1.0459 ^a	1.72	1.17	0.65
0955+476	1.882	18.9	1.0291 ^a	2.44	1.63	< 0.17
0957+003	0.905	19.3	0.6722 ^a	1.85	1.32	0.33
1005–333	1.837	18.0 [†]	1.3734 ^b	0.93	0.84	–
1012+022	1.375	17.3	0.7632 ^a	1.60	0.76	0.29
1011+280	0.899	18.6 [*]	0.8895 ^g	> 2	1.46	–
1116+128	2.129	18.9	0.5163 ^a	2.48	0.61	< 0.15
1116+128	2.129	18.9	0.6346 ^a	0.92	–	0.40
1136+408	2.366	20.0	1.3702 ^a	1.61	0.82	< 0.13
1142+052	1.345	19.5	1.3431 ^a	2.21	1.32	1.05
1200+068	2.182	19.8 [‡]	0.862 ^h	5.57	3.75	2.98
1204+399	1.518	19.0	1.3254 ^a	1.22	0.61	< 0.12
1210+134	1.139	18.4	0.7717 ^a	1.26	0.75	0.32
1222+438	1.075	19.7	0.7033 ^a	1.51	1.29	< 0.24
1226+105	2.307	19.1	0.9382 ^a	1.69	0.78	0.33
1318–263	2.027	21.3 [†]	1.1080 ^b	1.38	0.61	0.49
1324–047	1.882	19.8 [†]	0.7850 ^b	2.58	1.77	0.73
1343+386	1.852	18.4	0.8076 ^a	1.50	1.03	< 0.13
1402–012	2.518	18.0 [†]	0.8901 ^b	1.21	0.99	0.19
1430–178	2.331	19.4 [†]	1.3269 ^a	0.60	0.45	0.32
1602+241	2.531	19.0	1.5246 ^a	1.50	1.23	0.72
1611+343	1.397	17.5	0.6672 ^a	1.36	0.58	0.15
1625+262	1.656	18.7	1.0156 ^a	1.43	0.73	0.22
1629+120	1.792	18.4 [*]	0.9004 ^d	1.06	0.63	–
1634+213	1.802	19.6	0.8001 ^a	2.60	1.56	0.73
1701+593	1.798	19.6	0.7238 ^a	1.86	1.06	0.45
2003–025	1.457	19.0 [*]	1.2116 ^e	2.65	1.27	< 0.31
2003–025	1.457	19.0 [*]	1.4106 ^e	0.74	0.34	–
2149+212	1.538	19.0 [*]	0.9115 ^d	0.72	0.95	0.34
2149+212	1.538	19.0 [*]	1.0017 ^d	2.46	1.0	< 0.15
2149–307	2.345	18.4 [†]	1.0904 ^b	1.45	0.78	< 0.11
2149–307	2.345	18.4 [†]	1.6996 ^b	–	–	–
2337–011	2.085	17.8	1.3606 ⁱ	1.55	1.21	0.54
2355–106	1.639	19.3	1.1727 ^a	1.66	1.14	0.50

Table 1. The absorption systems: optical data. Typical errors on the rest equivalent widths are $\sim 0.05 - 0.1\text{\AA}$. Notes: [†]B-magnitude, from the APM catalogue or Jackson et al. (2002); ^{*}V-magnitude, from RTN06 or the NASA/IPAC Extragalactic Database; [‡]g-magnitude, from the SDSS; References for redshifts and equivalent widths: (a) SDSS DR-5 catalogue; (b) Ellison et al. (2004); (c) Sargent et al. (1988); (d) Barthel et al. (1990); (e) Aldcroft et al. (1994); (f) Sargent et al. (1989); (g) Peterson & Strittmatter (1978); (h) Wild & Hewett (2005); (i) Khare et al. (2004); (j) Steidel & Sargent (1992); (k) York et al. (2007).

DLAs with high spin temperatures and/or low covering factors² would remain undetected at such a sensitivity. Note that fewer than 5% of Galactic sightlines have $[T_s/f] > 1000$ K (see Fig. 2 of Braun & Walterbos 1992).

Our search for H I 21cm absorption was hence aimed at achieving an H I 21cm optical depth sensitivity of $\tau_{3\sigma} \sim 0.01$ per ~ 10 km s⁻¹ for all non-detections, so as to detect all DLAs with $[T_s/f] \lesssim 1000$ K. Absorbers with high H I column densities or low spin temperatures would be detected at higher significance.

The practical effect of the above sensitivity criterion was that the background quasars were chosen to have flux densities $S_\nu \gtrsim 300$ mJy at the redshifted H I 21cm line frequency, to ensure a high optical depth sensitivity in a reasonable integration time ($\lesssim 10$ hours). In most cases, the quasar flux densities had not been measured at (or near) the expected H I 21cm line frequency; we hence estimated the flux density at the line frequency by interpolating between measurements at higher and lower frequencies, using radio surveys such as the 1.4 GHz NRAO VLA Sky Survey (NVSS; Condon et al. 1998), the 1.4 GHz VLA FIRST Survey (Faint Images of the Radio Sky at Twenty Centimeter; Becker et al. 1995), the 327 MHz Westerbork Northern Sky Survey (WENSS; Rengelink et al. 1997) or the 365 MHz Texas Survey (Douglas et al. 1996).

A few quasars with lower flux densities, but having foreground MgII absorbers with $W_0^{12796} \geq 0.5\text{\AA}$, were also observed, especially when data towards the primary targets were affected by RFI. We also observed one absorber, at $z_{\text{abs}} \sim 1.6996$ towards 2149–307 (Ellison & Lopez, *in prep.*), where the MgII λ 2796 transition has not been observed, but which shows strong metal lines, and is hence likely to be a strong MgII absorber.

Our final absorber sample consists of 55 systems, at $0.58 < z_{\text{abs}} < 1.70$. Details of the absorbers and their background quasars are provided in Table 1, whose columns contain (1) the quasar name, (2) the quasar redshift, (3) the quasar R-magnitude (but see the notes to the table), (4) the MgII λ 2796 absorption redshift (or metal-line redshift, for the $z_{\text{abs}} \sim 1.6996$ absorber towards 2149–307), (5) the MgII λ 2796 rest equivalent width, W_0^{12796} , (6) the FeII λ 2600 rest equivalent width, W_0^{12600} , and (7) the MgI λ 2852 rest equivalent width, W_0^{12852} . Most absorbers of the sample have $W_0^{12600} \geq 0.5\text{\AA}$, while typical errors on the rest equivalent widths are ~ 0.05 – 0.1\AA . We emphasize that our MgII absorber sample is a heterogeneous one, drawn from different surveys with very different selection criteria.

3 OBSERVATIONS AND DATA ANALYSIS

The GMRT and GBT searches for redshifted H I 21cm absorption were carried out between January 2002 and September 2008. 14 systems at $1.12 < z_{\text{abs}} < 1.54$, for which the redshifted H I 21cm absorption frequency lies in the GMRT 610 MHz band (~ 560 – 670 MHz) were observed with the GMRT (proposals 07NKA02, 10NKA01, 10NKA02, 11NKA02, 12NKA01), due to its better RFI environment and superior spectral baselines; the remaining 41 targets were observed with the PF1-600, PF1-800 or PF2 receivers of the GBT (proposals 6A-026, 6C-048 and 7B-007).

3.1 GMRT observations and data analysis

The GMRT observations used the 30-station FX correlator as the backend, with two circular polarizations and a bandwidth of 0.5 or 1 MHz sub-divided into either 128 or 256 channels, yielding a velocity resolution of ~ 2 – 8 km s⁻¹. The standard calibrators 3C147, 3C286, or 3C48, were used to calibrate the flux density scale and usually also to determine the shape of the passband. Observations of target sources were interleaved (at ~ 45 -minute intervals) with short observations of nearby phase calibrators to obtain an initial estimate of the antenna gains. Our experience with the GMRT indicates that the flux density calibration is reliable to better than $\sim 15\%$ in this observing mode.

The GMRT data were analysed in “classic” AIPS, using standard procedures. After initial editing of corrupted data (e.g. due to “dead” antennas, correlator errors, RFI, etc), the antenna gains and bandpass shapes were determined using the calibrator data. A continuum image was then made of each target field (after averaging line-free channels to increase the signal-to-noise ratio) and self-calibration procedures used to obtain a better estimate of the antenna gains. Three or four iterations of phase self-calibration, followed by one or two of amplitude & phase self-calibration (along with further editing of bad data), were typically found necessary to obtain convergent antenna gains; the source flux density was then measured from the final image. The continuum emission was next subtracted out from the calibrated visibilities, using the task UVSUB (followed, in some cases, by the task UVLIN, to remove any residual emission). For all antenna baselines, the residual visibilities were then inspected in the time-frequency plane (using the task SPFLG) and any channel-dependent RFI was edited out. Finally, the edited residual visibilities were imaged in all channels to produce a spectral cube. The target sources were usually unresolved (or, in a few cases, marginally resolved) by the GMRT synthesized beam and a single spectrum was hence extracted in each case from the final spectral cube at the source location. Typically, a second-order baseline was subtracted from this, using line-free channels, to produce the final spectrum for each source.

3.2 GBT observations and data analysis

The GBT observations (in projects 6A-026, 6C-048 and 7B-007) usually used the Spectral Processor as the backend, due to its high dynamic range, with two linear polarizations. The observing bandwidths were 1.25 or 2.5 MHz, sub-divided into 1024 channels, yielding spectral resolutions of ~ 1 – 2 km s⁻¹ after Hanning smoothing. Five of the observing sessions (in one of which the two MgII absorbers towards 0240–060 were observed simultaneously) used the Auto-Correlation Spectrometer as the backend, as the Spectral Processor was not available. These had a bandwidth of 12.5 MHz, sub-divided into 32768 channels, yielding a spectral resolution of ~ 0.3 km s⁻¹ after Hanning smoothing (with 16384 channels and ~ 0.6 km s⁻¹ for each spectrum towards 0240–060). All GBT observations were carried out in position-switched, total power mode, with online system temperature measurements obtained by firing a noise diode.

The GBT data were analysed in DISH, the AIPS++ single-dish package. Much editing was usually necessary to remove data corrupted by RFI. Despite this, data on 13 sources could not be salvaged, due to strong RFI at or near the observing frequency. For the remaining sources, after the initial editing and calibration, the continuum flux density was first measured using RFI- and line-free channels. A first- or second-order baseline (determined by in-

² The covering factor f gives the fraction of quasar radio flux density occulted by the foreground absorber.

QSO	z_{abs}	Tel.	ν_{obs} MHz	BW MHz	Resn. km s ⁻¹	Time Hrs.	S_{ν} Jy	RMS ^a mJy	$\int \tau dV$ km s ⁻¹	T_s/f [†] K	N_{HI} [†] $\times 10^{20}$ cm ⁻²	α	
0017+154	1.6260	GBT	540.90	1.25	1.4	0.8	7.3	27.2	< 0.045	> 2500	< 0.8	-1.08	Y
0039-407	0.8483	GBT	768.49	2.5	1.9	3.5	0.11	3.7	< 0.49	> 225	< 8.9	+0.50	N
0014+813	1.1109	GBT	672.89	2.5	2.2	0.7	RFI	—	—	—	—	+0.00	R
0014+813	1.1125	GBT	672.38	2.5	2.2	0.7	RFI	—	—	—	—	+0.00	R
0105-008	1.3710	GMRT	599.07	1.0	2.0	3.5	1.26	3.3	0.995 ± 0.023	110 ± 3	18.14 ± 0.41	-0.32	A
0109+176	0.8392	GBT	772.30	2.5	1.9	4.2	1.5	4.3	< 0.039	> 2855	< 0.7	-0.97	Y
0237-233	1.3647	GMRT	600.67	1.0	3.9 ^b	12	5.53	2.5	< 0.014	> 6665	< 0.3	+0.55	Y
0237-233	1.6724	GBT	531.51	0.625	0.69	1.5	6.7	55.9	0.076 ± 0.016	1440 ± 300	1.39 ± 0.29	+0.55	Y
0240-060	0.5810	GBT	898.42	12.5 ^c	0.51	4.3	0.66	4.5	< 0.075	> 1430	< 1.4	+0.27	Y
0240-060	0.7550	GBT	809.35	12.5 ^c	0.57	4.3	0.65	3.7	< 0.061	> 1820	< 1.1	+0.27	Y
0244-128	0.8282	GBT	776.94	1.25	0.94	2.2	0.55	6.5	< 0.13	> 835	< 2.4	-0.32	Y
0311+430	1.068	GBT	686.85	1.25	1.1	2.3	4.55	10.3	< 0.03	> 3335	< 0.6	-1.06	Y
0409-045	0.8797	GBT	755.66	2.5	1.9	2.5	0.41	4.5	< 0.14	> 800	< 2.5	-0.79	Y
0445+097	0.8392	GBT	772.30	2.5	1.9	1.8	2.0	5.9	< 0.054	> 2000	< 1.0	-0.74	Y
0458-020	1.5605	GBT	554.74	1.25	1.3	4.5	2.2	8.2	0.161 ± 0.015	685 ± 65	2.93 ± 0.28	-0.07	Y
0642+449	1.2468	GMRT	632.19	1.0	7.8	6.0	0.35	1.0	< 0.09	> 1250	< 1.6	+0.04	Y
0741+294	1.0625	GBT	688.68	2.5	2.1	1.7	0.59	16.8	< 0.56	> 200	< 10	-0.62	N
0801+303	1.1908	GMRT	648.35	1.0	3.6 ^b	5.0	2.07	2.2	0.305 ± 0.025	360 ± 30	5.56 ± 0.46	-0.74	Y
0804+499	1.4071	GMRT	590.09	1.0	4.0	3.3	0.68	2.8	< 0.13	> 835	< 2.4	-0.97	Y
0812+332	0.8518	GBT	767.04	2.5	1.9	2.0	0.76	4.9	< 0.11	> 1000	< 2.0	-0.62	Y
0821+394	1.0545	GBT	691.36	1.25	1.1	0.5	5.2	20.0	< 0.053	> 2000	< 1.0	-0.67	Y
0829+425	1.0459	GBT	694.27	2.5	2.1	1.2	RFI	—	—	—	—	-0.60	R
0955+476	1.0291	GBT	700.02	1.25	1.1	2.0	1.4	11.5	< 0.12	> 950	< 2.1	+0.48	Y
0957+003	0.6722	GBT	849.42	2.5	1.7	0.6	2.2	9.8	< 0.06	> 1820	< 1.1	-0.90	Y
1005-333	1.3734	GBT	598.47	1.25	1.2	0.8	1.8	17.4	< 0.11	> 950	< 2.1	-0.82	Y
1012+022	0.7632	GBT	805.58	12.5 ^c	0.29	0.7	2.2	17.9	< 0.06	> 1665	< 1.2	-0.82	Y
1011+280	0.8895	GBT	751.74	12.5 ^c	0.30	1.2	RFI	—	—	—	—	-0.87	R
1116+128	0.5163	GBT	936.76	12.5 ^c	0.25	0.1	RFI	—	—	—	—	-0.90	R
1116+128	0.6346	GBT	868.96	12.5 ^c	0.27	0.1	RFI	—	—	—	—	-0.90	R
1136+408	1.3702	GMRT	599.28	1.0	3.9	2.3	0.49	2.6	< 0.13	> 910	< 2.2	-0.10	Y
1142+052	1.3431	GMRT	606.21	1.0	3.9	6.5	1.01	1.3	0.557 ± 0.030	195 ± 10	10.15 ± 0.55	-0.55	A
1200+068	0.862	GBT	762.84	2.5 ^d	1.9	2.2	0.79	3.8	< 0.08	> 1430	< 1.4	-0.45	Y
1204+399	1.3254	GMRT	610.82	1.0	3.8	3.0	0.38	2.7	< 0.23	> 475	< 4.2	-0.30	N
1210+134	0.7717	GBT	801.72	1.25	0.91	1.8	2.2	10.8	< 0.052	> 2220	< 0.9	-0.46	Y
1222+438	0.7033	GBT	833.91	2.5	1.8	2.2	0.19	4.8	< 0.42	> 260	< 7.7	-0.41	N
1226+105	0.9382	GBT	732.85	2.5	2.0	1.0	RFI	—	—	—	—	-0.82	R
1318-263	1.1080	GBT	673.82	1.25	1.1	0.7	RFI	—	—	—	—	-0.20	R
1324-047	0.7850	GBT	795.75	2.5	1.8	2.2	0.14	4.8	< 0.48	> 225	< 8.8	-0.57	N
1343+386	0.8076	GBT	785.80	1.25	0.93	1.3	1.7	7.4	< 0.06	> 1820	< 1.1	-0.52	Y
1402-012	0.8901	GBT	751.50	1.25	0.97	2.0	0.87	6.5	< 0.09	> 1175	< 1.7	+0.33	Y
1430-178	1.3269	GMRT	610.43	1.0	3.7	12	1.05	1.0	0.127 ± 0.022	860 ± 150	2.32 ± 0.40	-0.17	Y
1602+241	1.5246	GMRT	562.63	1.0	4.2	2.3	0.63	12.0	< 0.6	> 180	< 11	+0.23	N
1611+343	0.6672	GBT	851.97	1.25	0.86	0.3	5.7	26	< 0.09	> 1250	< 1.6	-0.63	Y
1625+262	1.0156	GBT	704.71	2.5	2.1	1.0	RFI	—	—	—	—	-0.94	R
1629+120	0.9004	GBT	747.43	2.5	2.0	1.2	RFI	—	—	—	—	-0.53	R
1634+213	0.8001	GBT	789.07	2.5	1.9	0.8	RFI	—	—	—	—	-0.32	R
1701+593	0.7238	GBT	824.00	2.5	1.8	2.0	0.76	4.5	< 0.1	> 1175	< 1.7	-0.89	Y
2003-025	1.2116	GMRT	642.25	1.0	7.2	8.0	3.4	2.4	< 0.022	> 5000 ^d	< 0.4 ^d	-0.48	Y
2003-025	1.4106	GMRT	589.23	1.0	4.0	15	3.7	2.8	0.210 ± 0.011	520 ± 25	3.83 ± 0.20	-0.48	Y
2149+212	0.9115	GBT	743.08	1.25	1.0	1.3	2.8	10.9	< 0.052	> 2220	< 0.9	-0.79	Y
2149+212	1.0017	GBT	709.60	2.5	2.1	1.8	RFI	—	—	—	—	-0.79	R
2149-307	1.0904	GBT	679.49	1.25	1.1	0.5	RFI	—	—	—	—	+0.21	R
2149-307	1.6996	GBT	526.15	1.25	1.4	2.5	1.6	13.9	< 0.12	> 910	< 2.2	+0.21	M
2337-011	1.3606	GMRT	601.71	0.5	1.9	15	0.063	1.9	2.04 ± 0.13	55 ± 2	37.2 ± 2.4	+0.73	Y
2355-106	1.1727	GMRT	653.75	1.0	1.8 ^b	4.0	0.42	2.5	0.256 ± 0.062	430 ± 55	4.67 ± 0.62	+0.62	Y

Table 2. Observing details and results. Notes to the table: [†]The quoted values of T_s/f and N_{HI} in columns (11) and (12) assume, respectively, an H I column density of 2×10^{20} cm⁻² and $T_s/f = 1000$ K; see the main text for discussion. ^aRMS noise at the Hanning-smoothed resolution of column (6). ^bThe spectrum was not Hanning-smoothed. ^cThese observations used the Auto-Correlation Spectrometer as the Spectral Processor was not available. ^dThe observations of 1200+068 used two settings, with the final spectrum (details listed) obtained by smoothing to the coarser resolution and averaging.

specting the individual spectra) was then fitted to each record and subtracted out during the process of calibration. The residual data were then averaged together to obtain the final spectrum for each source. In the case of multiple observing epochs for a single source (sometimes with different observational parameters), the spectra were first smoothed to the same spectral resolution, then interpolated onto the same heliocentric frequency scale, and finally averaged, with appropriate weights derived from the noise values. A low-order polynomial (upto second order) was then subtracted from this, using line- and RFI-free channels, to produce the final spectrum for each absorber.

4 SPECTRA AND RESULTS

For optically-thin HI 21cm absorption against a radio-loud quasar, the HI column density, N_{HI} , HI 21cm optical depth, τ , and spin temperature, T_s , are related by the expression (e.g. Rohlfs & Wilson 2006)

$$N_{\text{HI}} = 1.823 \times 10^{18} \times [T_s/f] \times \int \tau dV, \quad (1)$$

where N_{HI} is in cm^{-2} , T_s in K, and the integral is over velocity, in km s^{-1} . For the general case of multi-phase gas along the line of sight, T_s is the column-density-weighted harmonic mean of the spin temperatures of the different phases. The covering factor f , the fraction of quasar radio flux density obscured by the foreground absorber, can be estimated by comparing the flux density measured at high spatial resolution [e.g. with very long baseline interferometry (VLBI) studies] with the total flux density of the quasar at the redshifted HI 21cm line frequency (e.g. Briggs & Wolfe 1983; Kanekar et al. 2007; Kanekar et al. 2009). While VLBI studies at frequencies < 1.4 GHz are not available in the literature for most of the quasars of our sample, higher-frequency VLBI observations (when available) will be used to estimate f and hence, to infer the HI column densities of the absorbers, using equation (1), for an assumed spin temperature of $T_s = 1000$ K.

The observational details and results are summarized in Table 2; the columns here contain (1) the quasar name, (2) the MgII λ 2796 absorption redshift z_{abs} , (3) the telescope used for the observations, (4) the redshifted HI 21cm frequency, in MHz, (5) the observing bandwidth, in MHz, (6) the velocity resolution, after Hanning smoothing, in km s^{-1} , (7) the on-source integration time, in hours, (8) the source flux density, in Jy, (9) the root-mean-square (RMS) noise, in mJy, (10) the integrated HI 21cm optical depth, $\int \tau dV$, in km s^{-1} , or, for non-detections, 3σ upper limits to the integrated HI 21cm optical depth, assuming a Gaussian profile with a full width at half maximum (FWHM) of 10 km s^{-1} , (11) the ratio $[T_s/f]$ derived from these observations, or 3σ lower limits to this quantity, assuming the DLA threshold HI column density of $2 \times 10^{20} \text{ cm}^{-2}$, (12) the HI column density inferred from the present observations, in units of $[T_s/1000] \times (1/f) \times 10^{20} \text{ cm}^{-2}$ (see equation 1), (13) the quasar spectral index, α , defined by $S_{\nu_1}/S_{\nu_2} = (\nu_1/\nu_2)^\alpha$ (for most sources of the present sample, $\nu_1 = 1.4$ GHz, and $\nu_2 = 365$ MHz), and (14) a letter indicating whether the absorber was included in the final sample (Y), or, if not, the reason for the exclusion, weak HI 21cm optical depth limit (N), RFI (R), associated MgII absorption (A), or unknown rest MgII λ 2796 equivalent width (M).

Eight definite detections (all with $> 5\sigma$ significance) of redshifted HI 21cm absorption, and one tentative detection (with $\sim 4.6\sigma$ significance), were obtained, at $1.17 \lesssim z_{\text{abs}} \lesssim 1.68$. Seven

of these were with the GMRT, three of which had been earlier independently found by Gupta et al. (2007), while two were with the GBT. All candidate HI 21cm absorbers were observed on multiple epochs to ensure that the spectral feature did not arise due to intermittent RFI. In most cases, the expected doppler shift in the topocentric line frequency (due to the motion of the Earth) was detected between the different observing epochs, confirming that the feature is likely to arise from an astronomical source. For the weak absorption feature at $z_{\text{abs}} \sim 1.3269$ towards 1430–178 (GMRT) and the tentative detection at ~ 1.6724 towards 0237–233, we have not detected the doppler shift, as the expected shift was very small ($< 5 \text{ km s}^{-1}$) between the different observing sessions. However, the HI 21cm line in the former system was detected at the same heliocentric frequency on two observing epochs separated by ~ 2 years, and is hence unlikely to arise due to RFI. The nine HI 21cm absorption profiles are shown in Fig. 1, in order of increasing absorption redshift, with individual systems discussed in the next section.

As mentioned earlier, the GBT spectra of 13 sources, mostly at $z_{\text{abs}} \sim 1$, were affected by strong RFI and did not prove useful; these are indicated by the label “RFI” in column (8) of Table 2. No evidence for absorption was seen at (or near) the expected redshifted HI 21cm frequency in the spectra of 32 sources, yielding (mostly) strong upper limits on the HI 21cm optical depth and the HI column density [see columns (10) and (11) of Table 2]. The spectra of the non-detections are shown in Fig. 2, in order of increasing absorption redshift.

After excluding the 13 systems affected by RFI and the $z_{\text{abs}} \sim 1.6996$ absorber towards 2149–307 (in which the MgII λ 2796 transition has not so far been observed), our sample consists of 41 strong MgII λ 2796 absorbers, at $0.58 < z_{\text{abs}} < 1.68$. Our observing goal was to achieve an optical depth sensitivity of $\tau_{3\sigma} \sim 0.01$ per $\sim 10 \text{ km s}^{-1}$ for all non-detections. In practice, we either detected HI 21cm absorption or achieved $\tau_{3\sigma} < 0.013$ per $\sim 10 \text{ km s}^{-1}$ for 35 of the above 41 targets. For six absorbers, our optical depth sensitivity was only $\tau_{3\sigma} \sim 0.02 - 0.06$, typically because the background quasar has a low flux density at the redshifted HI 21cm line frequency or because a significant fraction of the data were affected by RFI. We will exclude these six systems from later statistical analysis due to the lower sensitivity of their HI 21cm spectra, so as to obtain a uniform optical depth criterion, $\tau_{3\sigma} < 0.013$. In addition, two systems (towards 0105–008 and 1142+052) lie within 3000 km s^{-1} of the background quasar and are thus “associated” absorbers. Following the general practice in the literature (e.g. Wolfe et al. 1986; Ellison et al. 2001), these are excluded from our statistical sample, as conditions in the absorbing gas could be affected by the presence of the nearby active galactic nucleus. These criteria imply that all “non-associated” DLAs with $[T_s/f] \lesssim 800$ K that are present in our statistical sample of 33 systems would have been detected in HI 21cm absorption. Of course, absorbers with higher HI column densities or lower spin temperatures would have been detected at higher significance.

5 INDIVIDUAL SYSTEMS

In this section, we discuss physical conditions in a few absorbers of interest, the nine detections of HI 21cm absorption and a non-detection in the known DLA towards 2149+212 (RTN06).

(i) 0105–008, $z_{\text{abs}} \sim 1.3710$: The absorber redshift is only $\sim 660 \text{ km s}^{-1}$ blueward of the quasar redshift ($z_{\text{em}} \sim 1.374$, from the SDSS), making this an “associated” absorber; it also has a relatively

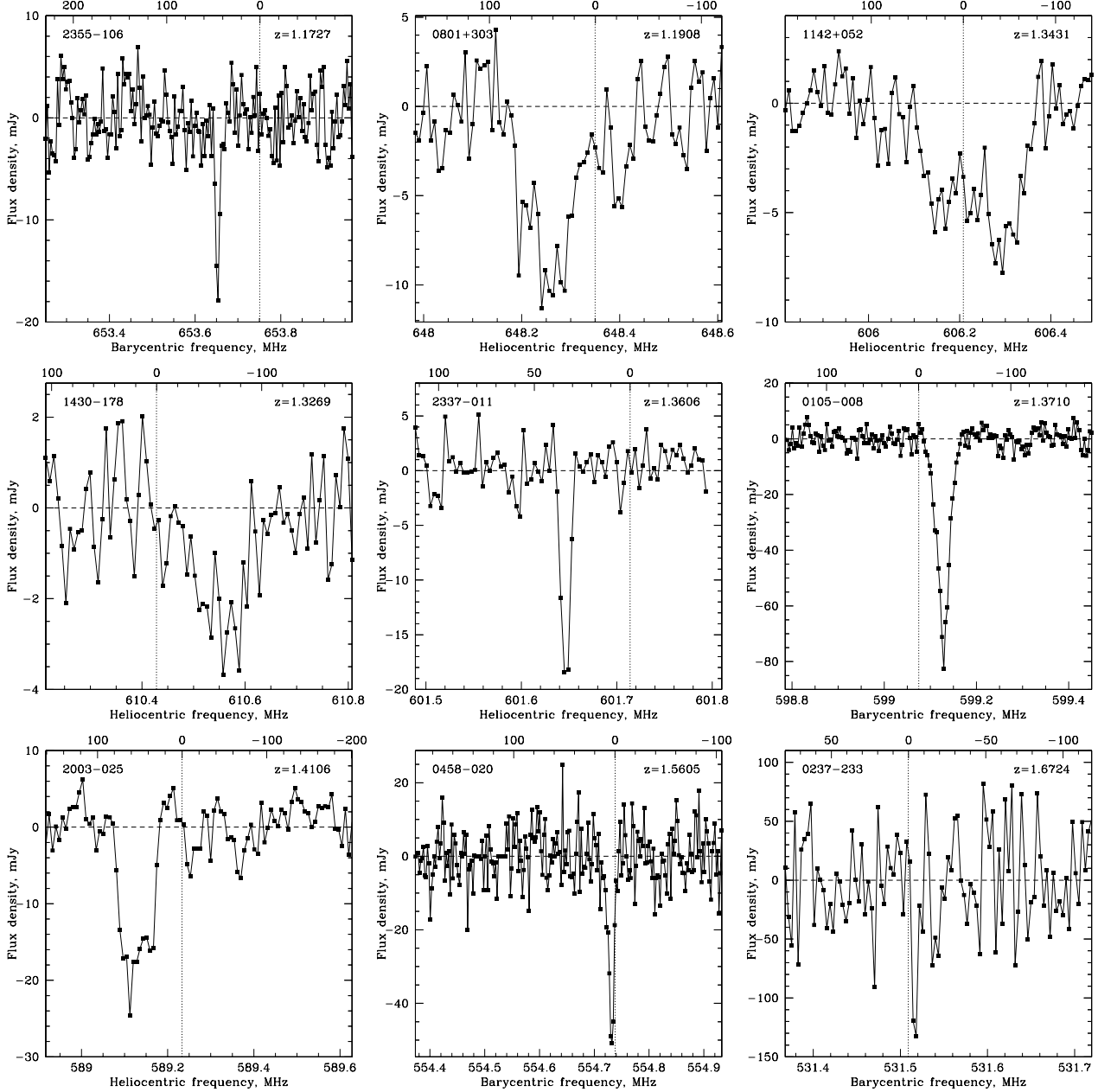


Figure 1. The GMRT and GBT spectra for the eight confirmed, and one tentative, detections of HI 21cm absorption, in order of increasing redshift. The MgII λ 2796 redshift is listed at the top right corner of each panel, and the expected HI 21cm line frequency indicated by the vertical dashed line. The velocity scale relative to the MgII λ 2796 redshift is indicated on the top axis of each panel.

low FeII λ 2600 rest equivalent width, $W_0^{\lambda 2600} = (0.38 \pm 0.05)\text{\AA}$. HI 21cm absorption from this system was originally detected by Gupta et al. (2007). Our new GMRT spectrum has a higher velocity resolution than the detection spectrum, and a slightly higher sensitivity. The peak optical depth in our spectrum matches that of Gupta et al. (2007). However, unlike them, we find that a single Gaussian component does not provide a good fit to the spectrum; two components, with FWHMs of $\sim (10.2 \pm 2.2) \text{ km s}^{-1}$ and $\sim (20.4 \pm 2.0) \text{ km s}^{-1}$, are needed to obtain residuals consistent with noise. The kinetic temperatures of the two components inferred from these FWHMs are $T_k \leq (2275 \pm 980) \text{ K}$ and

$T_k \leq (9095 \pm 1785) \text{ K}$.³ Only $\sim 30\%$ (170 mJy) of the total 2.3 GHz quasar flux density ($\sim 0.58 \text{ Jy}$) is recovered in a Very Long Baseline Array (VLBA) 2.3 GHz image [from the VLBA Calibrator Survey (VCS); Beasley et al. 2002], indicating that significant flux density is present in extended emission. The covering factor is hence likely to be low, < 0.3 at the redshifted HI 21cm line frequency. The

³ Note that $T_k \approx T_s$, for a single cold cloud (e.g. Liszt 2001). However, the kinetic temperature of an individual cold cloud in a DLA would typically be lower than the estimated absorber spin temperature, due to the presence of warm HI along the line of sight.

HI 21cm column density of the absorber thus appears quite high, $N_{\text{HI}} \sim (6.05 \pm 0.14) \times [T_s/1000] (0.3/f) \times 10^{21} \text{ cm}^{-2}$.

(ii) 0458–020, $z_{\text{abs}} \sim 1.5605$: The GBT HI 21cm profile is well fit by a single Gaussian component, with FWHM $\sim (6.48 \pm 0.76) \text{ km s}^{-1}$; the upper limit to the gas kinetic temperature is thus $(915 \pm 215) \text{ K}$. Briggs et al. (1989) used VLBI studies at 327, 467 and 608 MHz to find that the central core-jet structure has a flux density of $\sim 1.8 \text{ Jy}$ at 608 MHz on scales $< 0.1''$, with a spectral index of $\alpha \sim +1.7$ between 467 and 608 MHz. This implies a compact flux density of $\sim 1.55 \text{ Jy}$ at the redshifted HI 21cm line frequency of 554.7 MHz, giving a covering factor $f > 0.7$. The HI column density of the absorber is thus $N_{\text{HI}} \sim (4.19 \pm 0.40) \times [T_s/1000] (0.7/f) \times 10^{20} \text{ cm}^{-2}$. This line of sight also contains another HI 21cm absorber, at $z_{\text{abs}} \sim 2.03945$ (Wolfe et al. 1985).

(iii) 0801+303, $z_{\text{abs}} \sim 1.1908$: Gupta et al. (2007) detected HI 21cm absorption from this absorber, but found differences between spectra taken at different epochs (probably due to low-level RFI), and were hence unable to confirm the presence of wide absorption or determine the velocity width of the line. We clearly detect wide HI 21cm absorption, obtaining a total velocity spread (full width between nulls, FWBN) of $\sim 125 \text{ km s}^{-1}$. The covering factor is again likely to be low: Kunert et al. (2002) find that only 456 mJy of the 1.6 GHz flux density is associated with the compact core, while the total 1.4 GHz flux density was measured to be 1.27 Jy in the NVSS. While both the core and the extended emission have steep spectra (Kunert et al. 2002), the covering factor at the redshifted HI 21cm line frequency of 648.35 MHz is likely to be lower than the 1.4 GHz core fraction, i.e. $f < 0.35$. The HI column density is $N_{\text{HI}} = (1.59 \pm 0.13) \times [T_s/1000] (0.35/f) \times 10^{21} \text{ cm}^{-2}$.

(iv) 1142+052, $z_{\text{abs}} \sim 1.3431$: The HI 21cm (and MgII) absorption arise within $\sim 40 \text{ km s}^{-1}$ of the QSO redshift ($z_{\text{em}} \sim 1.3425$), implying that this is also an “associated” system; the absorption may originate in the quasar host galaxy. The HI 21cm profile is quite wide, with FWBN $\sim 145 \text{ km s}^{-1}$. Again, the absorber covering factor is likely to be low at the redshifted HI 21cm line frequency; only $\sim 30\%$ of the total 2.3 GHz quasar flux density ($\sim 0.6 \text{ Jy}$) is recovered in the VCS image (Beasley et al. 2002). The HI column density is $N_{\text{HI}} = (3.38 \pm 0.18) \times [T_s/1000] (0.3/f) \times 10^{21} \text{ cm}^{-2}$.

(v) 1430–178, $z_{\text{abs}} \sim 1.3269$: This is the weakest absorption line of our sample, with peak line depth $\sim 4 \text{ mJy}$. The HI 21cm absorption is again quite wide, with FWBN $\sim 115 \text{ km s}^{-1}$. The 2.3 GHz VCS image finds a quasar flux density of $\sim 0.46 \text{ Jy}$, $\sim 55\%$ of the total 2.3 GHz flux density (Beasley et al. 2002). The quasar also has a flat spectrum between 5 GHz and 408 MHz, suggesting that it is likely to be core-dominated. The covering factor at the redshifted HI 21cm frequency is thus likely to be similar to that at 2.3 GHz, i.e. $f \sim 0.55$. The total HI column density is then $N_{\text{HI}} = (4.21 \pm 0.73) \times [T_s/1000] (0.55/f) \times 10^{20} \text{ cm}^{-2}$.

(vi) 2003–025, $z_{\text{abs}} \sim 1.4106$: The HI column density of this absorber has been measured to be $\log N_{\text{HI}} = (20.54^{+0.15}_{-0.24}) \times 10^{20} \text{ cm}^{-2}$, from the damped Lyman- α absorption profile (RTN06). The integrated HI 21cm optical depth of $(0.210 \pm 0.011) \text{ km s}^{-1}$ then gives a spin temperature of $T_s = (905 \pm 380) \times f \text{ K}$, where the error is dominated by that on the HI column density. Unfortunately, no VLBI observations of the background quasar are available in the literature; it is thus not possible to estimate the covering factor. We note that the quasar is unresolved by the GMRT synthesized beam (of angular size $\sim 7''.1 \times 5''.3$) and is hence likely to be compact. This absorber has a low FeII $\lambda 2600$ rest equivalent width, $W_0^{\lambda 2600} = (0.34 \pm 0.08) \text{ \AA}$.

(vii) 2149+212, $z_{\text{abs}} \sim 1.1727$: This is another known DLA, with an HI column density of $\log N_{\text{HI}} = 20.70^{+0.08}_{-0.10}$ (RTN06). Equation 1 then yields $T_s > (2700 \times f) \text{ K}$. No VLBI information on the quasar is available in the literature and it is hence not possible to estimate its covering factor.

(viii) 2337–011, $z_{\text{abs}} \sim 1.3606$: This absorber has the highest peak HI 21cm optical depth of our sample, $\tau_{\text{peak}} \sim 0.35$. The HI 21cm line is quite narrow, and is well fit by a single Gaussian of FWHM $= (5.74 \pm 0.54) \text{ km s}^{-1}$; this implies an upper limit to the kinetic temperature of $(720 \pm 135) \text{ K}$. The background quasar has a highly inverted spectrum (spectral index $\alpha \sim +0.73$), and is clearly core-dominated. The covering factor is thus likely to be close to unity, especially in view of the high peak optical depth; formally, $f > 0.35$. The HI column density of the absorber is $N_{\text{HI}} = (3.72 \pm 0.24) \times [T_s/1000] (1/f) \times 10^{21} \text{ cm}^{-2}$, among the highest in our sample.

(ix) 2355–106, $z_{\text{abs}} \sim 1.1727$: The HI 21cm absorption in this system was originally detected by Gupta et al. (2007); our new GMRT spectrum has similar sensitivity and velocity resolution. As noted by Gupta et al. (2007), a single Gaussian provides a good fit to this profile; we obtain a peak optical depth of (0.043 ± 0.005) and FWHM $= (5.03 \pm 0.73) \text{ km s}^{-1}$, slightly deeper and narrower than that of Gupta et al. (2007), but consistent within the errors. Gupta et al. (2007) argue for a high covering factor, based on the compactness of the source in a 5 GHz VLBA image (Fomalont et al. 2000). Similarly, a 2.3 GHz VCS image recovers $\sim 90\%$ of the total 2.3 GHz quasar flux density (Beasley et al. 2002), and the source has a highly inverted spectrum, indicating that it is core-dominated. The covering factor is thus likely to be ~ 0.9 at the redshifted HI 21cm line frequency, yielding an HI column density of $N_{\text{HI}} = (5.18 \pm 0.19) \times [T_s/1000] (0.9/f) \times 10^{20} \text{ cm}^{-2}$.

(x) 0237–233, $z_{\text{abs}} \sim 1.6724$: The absorption feature was seen in data from two separate GBT observing sessions in November 2006, close to the expected redshifted HI 21cm line frequency from the MgII redshift. Although attempts were made to confirm the line in August 2008 with the GBT, the RFI environment at these frequencies was found to have significantly deteriorated and it was not possible to obtain useful data; we hence list this as a tentative detection. Srianand et al. (2007) discuss high-frequency (2.3–8.4 GHz) VLBI studies of this source from the literature (e.g. Fomalont et al. 2000) and conclude that most of the flux density arises from two components, separated by $\sim 10 \text{ mas}$. The lowest frequency at which a VLBI study has been carried out is 1.6 GHz, where Hodges et al. (1984) found no evidence for extended structure, obtaining a size of $\sim 6 \times 3 \text{ mas}$. The covering factor is thus likely to be high, $f \sim 1$. The tentative detection of HI 21cm absorption in this system yields the lowest HI column density of all our detections, $N_{\text{HI}} \sim (1.39 \pm 0.29) \times [T_s/1000] (1/f) \times 10^{20} \text{ cm}^{-2}$; note that the absorber must have a high spin temperature, if it is indeed a DLA.

6 EARLIER SEARCHES FOR HI 21CM ABSORPTION IN MgII-SELECTED SAMPLES

The criterion of MgII absorption has long been used as a criterion to select targets for searches for redshifted HI 21cm absorption (e.g. Roberts et al. 1976; Brown & Spencer 1979; Peterson & Foltz 1980), although these early studies typically observed few targets with relatively low sensitivity. The first survey for HI 21cm absorption in a sizeable sample of MgII absorbers was carried out by Briggs & Wolfe (1983), who used the Arecibo and NRAO 300-ft telescopes to target 15 MgII absorbers with $W_0^{\lambda 2796} \gtrsim 0.5 \text{ \AA}$ and

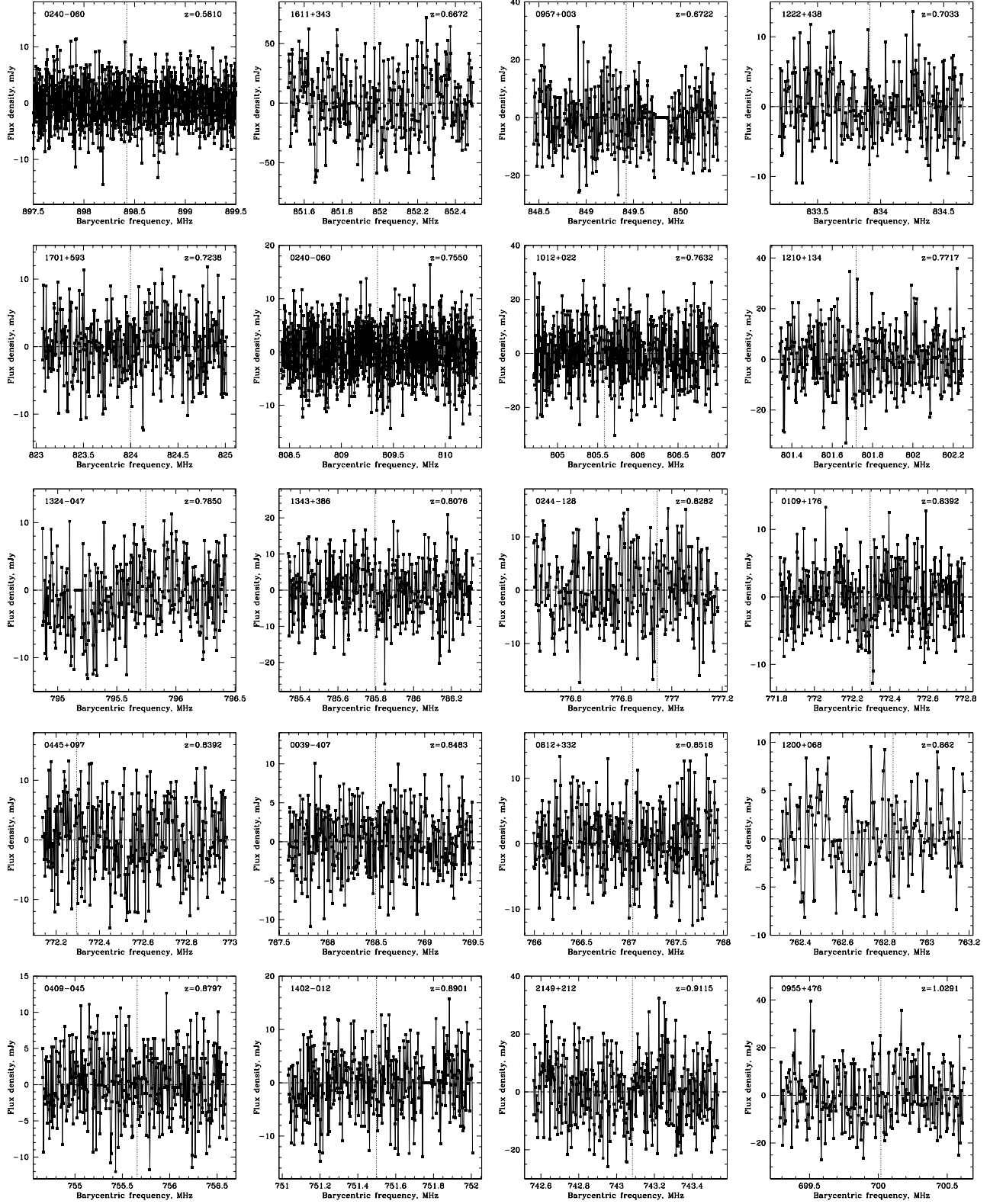


Figure 2. The GMRT and GBT spectra for the 35 non-detections of H I 21cm absorption, in order of increasing Mg II λ 2796 absorption redshift. The expected H I 21cm line frequency, based on the Mg II λ 2796 redshift, is indicated by the dashed line in each panel.

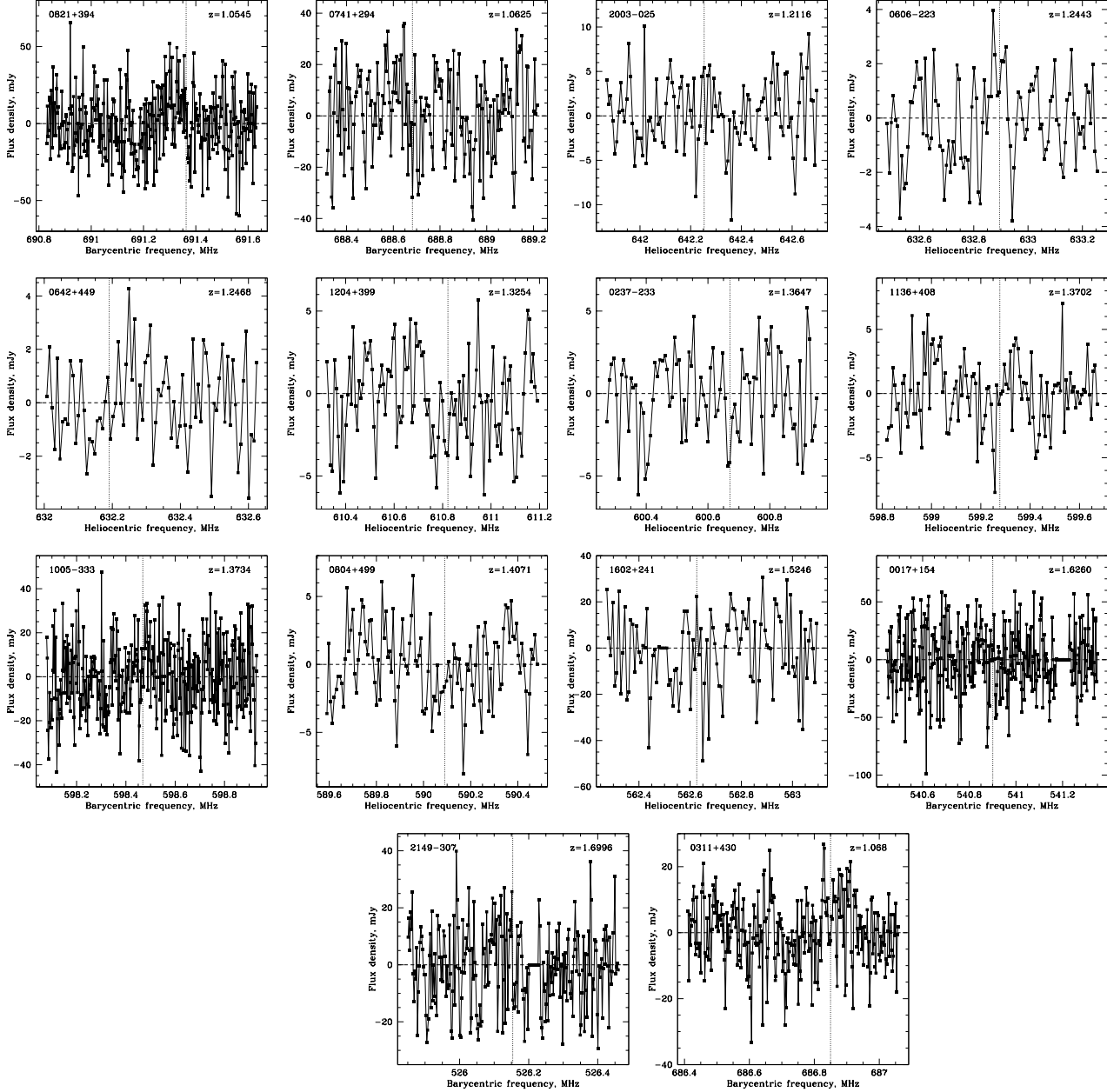


Figure 2. (continued).

$0.4 \lesssim z_{\text{abs}} \lesssim 1.8$. They obtained optical depth sensitivities of $\tau_{3\sigma} \sim 0.01 - 0.1$ per $\sim 10 \text{ km s}^{-1}$, but with no new detections of HI 21cm absorption.

More recently, Lane (2000) carried out a search for redshifted HI 21cm absorption in a large sample of MgII absorbers (62 systems, with $W_0^{12796} > 0.3\text{\AA}$ and at $0.2 < z_{\text{abs}} < 1$), using the Westerbork Synthesis Radio Telescope. While this survey observed significantly more targets than earlier studies, the mean 3σ optical depth sensitivity of $\tau_{3\sigma} \sim 0.048$ was only sufficient to detect strong HI 21cm absorbers, resulting in four new detections, all at $z_{\text{abs}} < 0.44$ (Lane et al. 1998; Lane 2000; Lane & Briggs 2001). Indeed, four systems that were not detected in HI 21cm absorption by Lane (2000) were later detected by deeper searches (Kanekar & Chengalur 2001, 2003; Curran et al.

2007), that achieved sensitivities of $\tau_{3\sigma} \lesssim 0.01$ per $\sim 10 \text{ km s}^{-1}$. The optical depth sensitivity of Lane (2000) was also typically lower for absorbers at $z_{\text{abs}} \gtrsim 0.6$ than for the low- z systems in their sample.

Gupta et al. (2007) used the GMRT to search for HI 21cm absorption in 10 strong MgII absorbers, at $1.11 < z_{\text{abs}} < 1.45$, obtaining three detections and seven upper limits to the HI 21cm optical depth. Their three absorption detections were observed during this survey and are included in our sample. Only one of their non-detections had an optical depth sensitivity $\tau_{3\sigma} \lesssim 0.01$ per $\sim 10 \text{ km s}^{-1}$; the remaining six had $\tau_{3\sigma} \sim 0.02 - 0.04$ per $\sim 10 \text{ km s}^{-1}$, in all cases worse than the sensitivity of our statistical sample ($\tau_{3\sigma} \leq 0.013$ per 10 km s^{-1}).

Finally, Srianand et al. (2008) report the detection of HI 21cm

Attribute	Median	H I 21cm detection rate, %	
		“High”	“Low”
W_0^{12796}	1.58 Å	17^{+16}_{-9}	33^{+20}_{-13}
W_0^{12600}	0.99 Å	22^{+18}_{-11}	28^{+19}_{-12}
W_0^{12852}	0.32 Å	29^{+20}_{-13}	18^{+17}_{-10}
W_0^{12796}/W_0^{12600}	1.49	18^{+17}_{-10}	33^{+20}_{-13}
α	-0.47	39^{+21}_{-14}	11^{+15}_{-7}
z_{abs}	1.04	50^{+23}_{-16}	0^{+10}

Telescope	No. of systems	H I 21cm detection rate, %
GMRT	12	58^{+31}_{-22}
GBT/Arecibo	24	8^{+11}_{-5}

Table 3. A comparison between the detection rates of H I 21cm absorption in different sub-samples. In the upper table, for each attribute (e.g. W_0^{12796} , W_0^{12600} , etc), the “High” and “Low” sub-samples consist of absorbers with attribute values higher and lower than the median, respectively.

absorption in two MgII absorbers at $z_{\text{abs}} \sim 1.3265$ towards SDSSJ0850+5159 and $z_{\text{abs}} \sim 1.3095$ towards SDSSJ0852+3435 with the GMRT. These were targetted based on the criterion $W_0^{12796} \geq 1\text{ Å}$, in a continuation of the survey of Gupta et al. (2007). Both absorbers have large metal line rest equivalent widths: the system at $z \sim 1.3265$ has $W_0^{12796} = 4.89\text{ Å}$, $W_0^{12852} = 2.08\text{ Å}$ and $W_0^{12600} = 2.27\text{ Å}$, while that at $z \sim 1.3095$ has $W_0^{12796} = 2.89\text{ Å}$, $W_0^{12852} = 1.11$ and $W_0^{12600} = 2.10\text{ Å}$.

We investigated the possibility of augmenting our statistical sample with H I 21cm results from these earlier studies. For this purpose, we required any such absorbers to satisfy the following constraints: (1) $W_0^{12796} \geq 0.5\text{ Å}$, (2) $0.58 \leq z_{\text{abs}} \leq 1.70$, (3) for non-detections, $\tau_{3\sigma} \leq 0.013$ per $\sim 10\text{ km s}^{-1}$, and (4) the velocity separation between the absorber and quasar redshifts should be $\geq 3000\text{ km s}^{-1}$. One system from the sample of Briggs & Wolfe (1983), at $z_{\text{abs}} \sim 0.8596$ towards 0454+039, fulfils all four conditions and was hence added to our sample. The detections of Gupta et al. (2007) were all observed in this search and are included here. The only other system from their sample that satisfies the sensitivity constraint is the $z_{\text{abs}} \sim 1.3647$ absorber towards 0237–233 (Srianand et al. 2007), for which we present a higher-sensitivity GMRT spectrum here. Both H I 21cm detections of Srianand et al. (2008) satisfy all our criteria and were added to the sample. Finally, no system from the sample of Lane (2000) satisfies all three constraints; most are ruled out by the sensitivity criterion.

7 THE INCIDENCE OF H I 21CM ABSORPTION IN STRONG MgII ABSORBERS

Including systems from the literature, our final statistical sample consists of 36 strong MgII absorbers at $0.58 < z_{\text{abs}} < 1.68$, with $W_0^{12796} \geq 0.57\text{ Å}$; the median MgII absorption redshift is $z_{\text{abs}} \sim 1.04$. 33 systems have $W_0^{12600} \geq 0.5\text{ Å}$, while three have either $W_0^{12600} < 0.5\text{ Å}$ (two absorbers) or no information on the FeII transition (the $z \sim 0.5810$ absorber towards 0240–060). There are nine

detections of H I 21cm absorption (including the tentative detection towards 0237–233) and 27 non-detections with $\tau_{3\sigma} \leq 0.013$ per $\sim 10\text{ km s}^{-1}$. Seven of the detections and 26 of the non-detections are from the present survey, with two detections from Srianand et al. (2008) and one non-detection from Briggs & Wolfe (1983). The median 3σ optical depth sensitivity for the non-detections is $\tau_{3\sigma} \sim 0.0062$ per $\sim 10\text{ km s}^{-1}$. The net detection rate of H I 21cm absorption is $25^{+11}_{-8}\%$ at a mean absorption redshift of $\bar{z} \sim 1.1$.⁴

We examined the data for correlations between the detection rate of H I 21cm absorption and the following set of absorber attributes: (1) W_0^{12796} , (2) W_0^{12600} , (3) W_0^{12852} , (4) W_0^{12796}/W_0^{12600} and (5) MgII absorption redshift. In order to test for possible systematic effects, we also checked whether the H I 21cm detection rate showed a dependence on the spectral index of the background quasar (which is indicative of the absorber covering factor) or the telescope used for the observations (interferometer versus single-dish). The small size of the full sample implies that, for any given attribute, it is only meaningful to divide the sample into two sub-samples at the median value of the quantity in question (except, of course, for the comparison between telescope types). This is the approach we will follow here.

Results of these comparisons are summarized in Table 3; the columns of the upper part of the table contain (1) the attribute used for the division (e.g. the MgII $\lambda 2796$ rest equivalent width, the quasar spectral index α , etc), (2) the median value of this attribute, (3) the detection rate of H I 21cm absorption for the “high” sample, with attribute values higher than the median (e.g. $\alpha > \alpha_{\text{med}}$), and (4) the detection rate for the “low” sample, with values lower than the median. For the lower half of the table, the columns are (1) the observing facility, divided into interferometers (GMRT) and single-dish telescopes (GBT and Arecibo), (2) the number of absorbers, and (3) the detection rates of H I 21cm absorption. No statistically-significant difference ($\geq 3\sigma$) is found between the detection rates in the sub-samples for any criterion, largely due to the small size of each sub-sample. For example, all nine detections of H I 21cm absorption were obtained at $z_{\text{abs}} > 1.04$, but the difference in detection rates in the high- z and low- z sub-samples has only $\sim 2.6\sigma$ significance. We conclude that the size of the present sample is too small to test the dependence of the detection rate on the properties of individual absorbers.

Finally, Figs. 3 and 4 show the integrated H I 21cm optical depth ($EW_{21} \equiv \int \tau dV$) plotted against W_0^{12796} , W_0^{12600} , W_0^{12852} , W_0^{12796}/W_0^{12600} , quasar spectral index α and MgII absorption redshift, for absorbers in the statistical sample. No statistically-significant correlation is found between EW_{21} and any of these quantities. However, it can be seen in Figs. 3[A–C] that a trend may be present between EW_{21} and each of W_0^{12796} , W_0^{12600} and W_0^{12852} , for detections of H I 21cm absorption. The possibility that a relation between EW_{21} and W_0^{12796} might be present only in the highest H I column density absorbers (i.e. DLAs) is explored further in the next section.

8 H I 21CM ABSORPTION IN DLAs

Very few DLAs with $0.8 \lesssim z_{\text{abs}} \lesssim 1.7$ are known towards radio-loud quasars, due to which there have been few H I 21cm absorption studies of systems in this redshift range. In fact, prior to this

⁴ All error bars correspond to 1σ Gaussian confidence levels, using small-number Poisson statistics (Gehrels 1986).

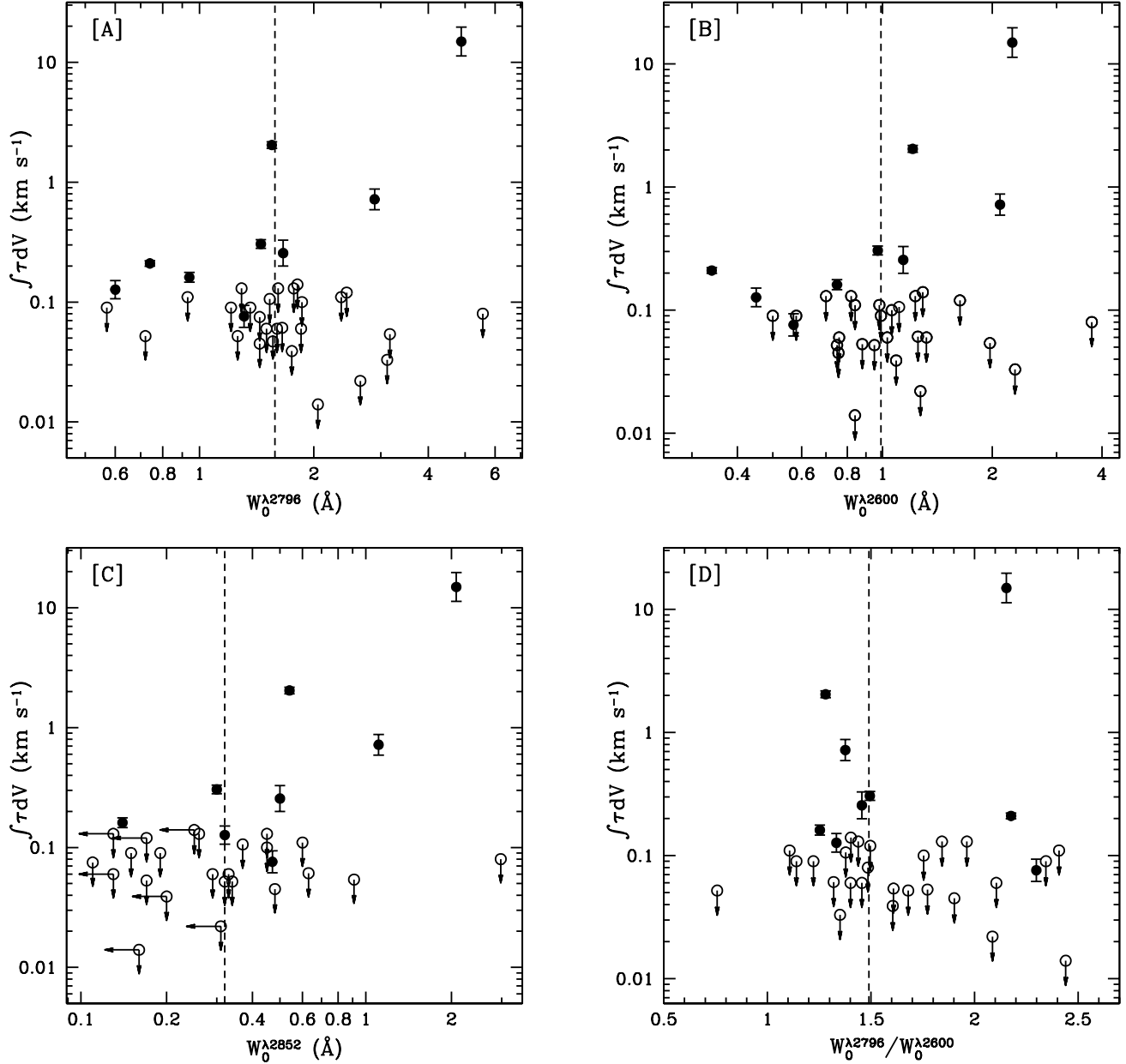


Figure 3. The four panels show the integrated HI 21cm optical depth plotted against (from top left) [A] the MgII λ 2796 rest equivalent width, [B] the FeII λ 2600 rest equivalent width (35 systems), [C] the MgI λ 2852 rest equivalent width (33 systems), and [D] $W_0^{\lambda 2796}/W_0^{\lambda 2600}$ (35 systems). Detections of HI 21cm absorption are shown as filled circles. The dashed vertical lines mark the median value of the quantity plotted as the abscissa in each panel.

$x_{21,\text{MgII}}(z)$	Detection rate of HI 21cm absorption in MgII λ 2796 absorbers
$x_{21,\text{DLA}}(z)$	Detection rate of HI 21cm absorption in DLAs
$x_{\text{DLA,MgII}}(z)$	Detection rate of DLAs in MgII λ 2796 absorbers
$n_{\text{DLA}}(z)$	Number of DLAs per unit redshift
$n_{\text{MgII}}(z, W_0)$	Number of MgII λ 2796 absorbers with $W_0^{\lambda 2796} \geq W_0$, per unit redshift

Table 4. Notation used in this paper.

work, only two “classical” DLAs (i.e. with $N_{\text{HI}} \geq 2 \times 10^{20} \text{ cm}^{-2}$) at these redshifts had been searched for HI 21cm absorption, with no detections (Kanekar & Chengalur 2003). The situation is quite different at both lower and higher redshifts. So far, six HI 21cm absorbers have been detected in “non-associated” DLAs at $z_{\text{abs}} \gtrsim 1.7$, with 12 limits on the HI 21cm optical depth (typically $\tau_{21} \sim 0.01$; e.g. Wolfe & Davis 1979; Wolfe et al. 1981, 1985; Kanekar & Chengalur 2003; Kanekar et al. 2006; York et al. 2007; Kanekar et al. 2007). The detection rate of HI 21cm absorption in high- z DLAs is thus $x_{21,\text{DLA}}(\bar{z} \sim 2.7) = 33^{+20}_{-13}\%$, where \bar{z} is the mean redshift of the DLA sample (see Table 4 for the notation used in this paper). Conversely, HI 21cm absorption has been detected in eleven DLAs at $z_{\text{abs}} < 0.9$, with

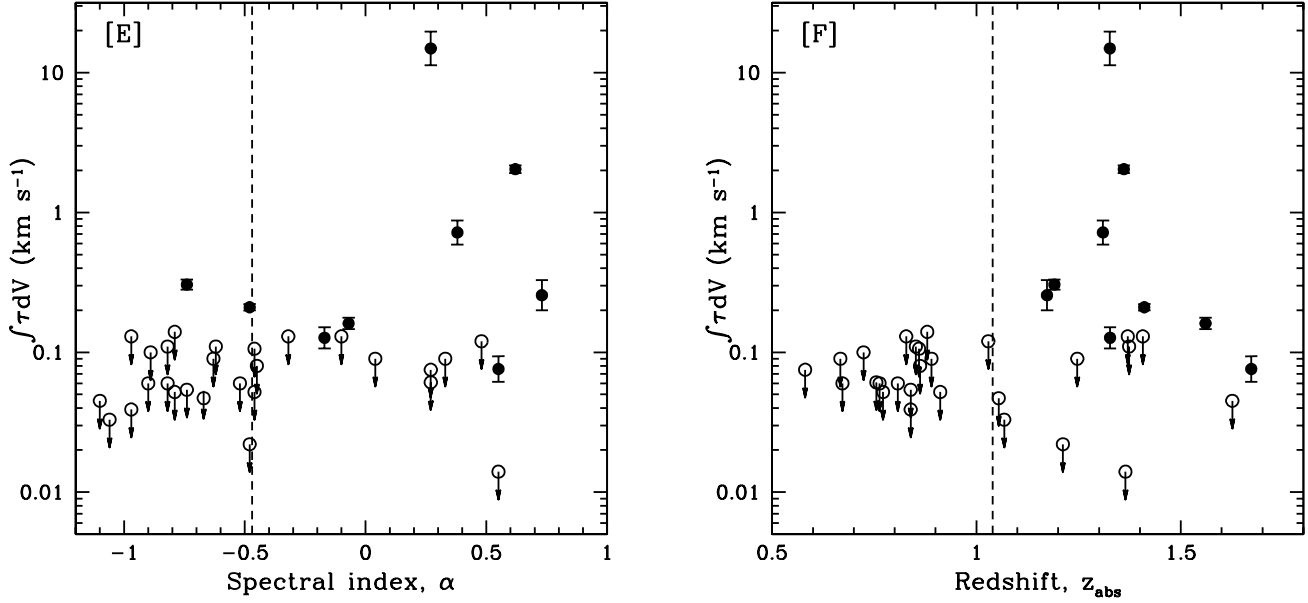


Figure 4. The two panels of the figure show the integrated H I 21cm optical depth plotted against [A] the low-frequency spectral index α of the background quasar, and [B] the absorber redshift, z_{abs} . Detections of H I 21cm absorption are shown as filled circles. The dashed vertical lines mark the median value of the quantity plotted as the abscissa in each panel.

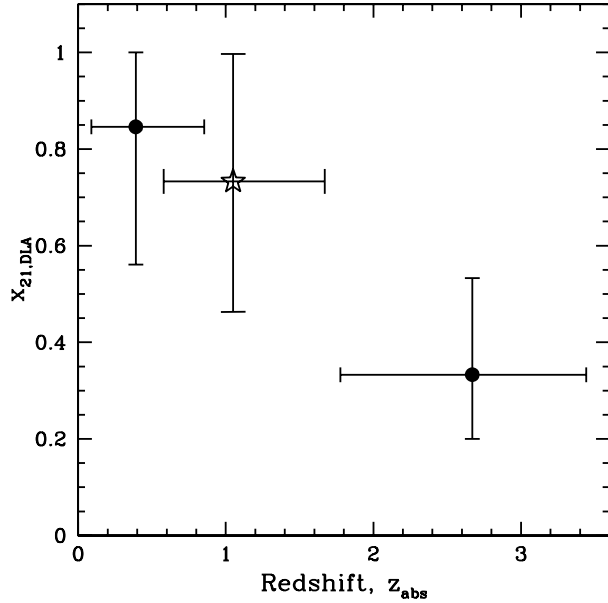


Figure 5. The detection rate of H I 21cm absorption in DLAs, plotted as a function of absorber redshift; the result from the present survey is shown as an open star. See the main text for discussion.

only two non-detections (e.g. Brown & Roberts 1973; Wolfe et al. 1976; Brown & Spencer 1979; Brown & Mitchell 1983; Lane et al. 1998; Chengalur & Kanekar 1999; Kanekar & Chengalur 2001; Curran et al. 2007). The detection rate of H I 21cm absorption in DLAs at $z_{\text{abs}} < 0.9$ is thus $x_{21,\text{DLA}}(\bar{z} \sim 0.4) = 85^{+15}_{-28}\%$. Recent low-frequency VLBI studies have shown that DLAs in the $z_{\text{abs}} > 1.7$ and $z_{\text{abs}} < 0.9$ samples have very similar covering factors, $0.4 < f < 1$ (Kanekar et al. 2007; Kanekar et al. 2009). The H I

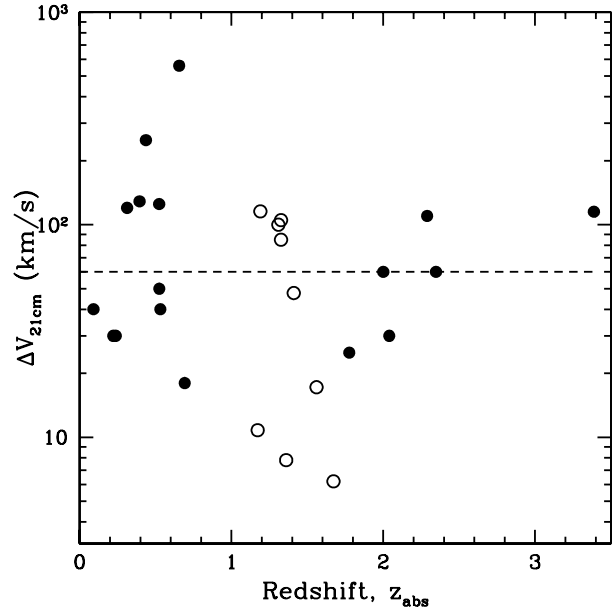


Figure 6. The velocity spread of H I 21cm absorption ΔV_{21} in strong MgII absorbers (in open circles) and DLAs (filled circles), plotted as a function of absorber redshift; the dashed line is at $\Delta V_{21} = 60 \text{ km s}^{-1}$.

column density distributions of the high- z and low- z DLA samples (with H I 21cm absorption studies) are also similar (Kanekar et al. 2009). The low detection rate of H I 21cm absorption in the high- z DLA sample is hence likely to be due to a higher fraction of warm H I in these absorbers (e.g. Wolfe & Davis 1979; Carilli et al. 1996; Kanekar & Chengalur 2003).

Our survey provides a direct estimate of the detection rate of H I 21cm absorption in strong MgII absorbers at $0.58 < z_{\text{abs}} < 1.68$.

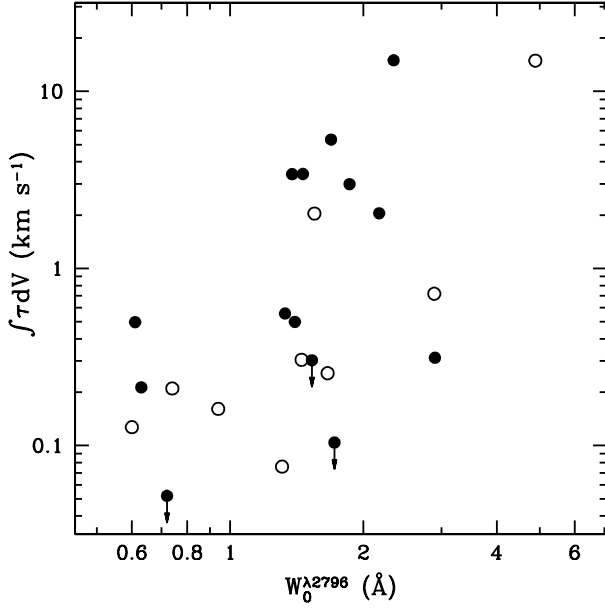


Figure 7. The integrated HI 21cm optical depth $EW_{21} \equiv \int \tau dV$ plotted against the rest equivalent width in the MgII $\lambda 2796$ transition, $W_0^{\lambda 2796}$, for HI 21cm absorbers and DLAs. Strong MgII absorbers with HI 21cm detections are shown as open circles, while DLAs from the literature are shown as filled circles. A trend between EW_{21} and $W_0^{\lambda 2796}$ is apparent in the figure, but has only $\sim 2.2\sigma$ significance in a non-parametric Kendall-tau test. See the main text for discussion.

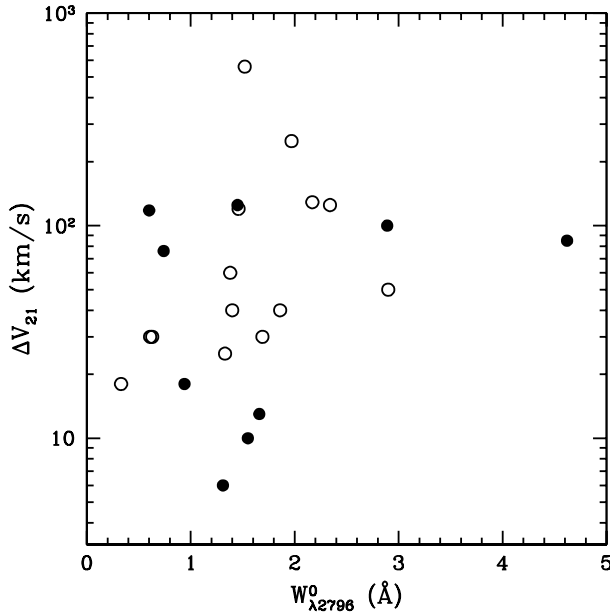


Figure 8. The velocity spread of HI 21cm absorption ΔV_{21} in strong MgII absorbers (open circles) and DLAs (filled circles), plotted as a function of the MgII $\lambda 2796$ rest equivalent width, $W_0^{\lambda 2796}$. See the main text for discussion.

We compute the HI 21cm detection rate in DLAs at these redshifts by taking the ratio of the detection rate in our sample to the detection rate of DLAs in MgII $\lambda 2796$ absorbers selected with the same criteria (RTN06).⁵ 35 of the 36 absorbers of our sample also have detected FeII $\lambda 2600$ absorption, with $W_0^{\lambda 2600} \geq 0.34 \text{\AA}$; we will use this 35-system sub-sample for the comparison with the DLAs of RTN06, applying the same selection criteria to their absorbers (i.e. $W_0^{\lambda 2796} \geq 0.57 \text{\AA}$, $W_0^{\lambda 2600} \geq 0.34 \text{\AA}$ and $0.58 \leq z_{\text{abs}} \leq 1.68$). There are 97 absorbers in the RTN06 sample that satisfy these selection criteria, of which 34 were found to be DLAs.

The probability that a strong MgII absorber is a DLA has been found to depend on the rest equivalent width of the MgII line, being higher for systems with higher values of $W_0^{\lambda 2796}$ (RTN06). We hence first tested whether our sub-sample of 35 absorbers with $W_0^{\lambda 2796} \geq 0.57 \text{\AA}$ and $W_0^{\lambda 2600} \geq 0.34 \text{\AA}$ has a similar distribution of $W_0^{\lambda 2796}$ values as the corresponding sub-sample of RTN06. A Kolmogorov-Smirnov rank-1 test finds a Gaussian probability of $\sim 24.5\%$ that the two samples are drawn from the same distribution of $W_0^{\lambda 2796}$ values, consistent with the null hypothesis within $\sim 1.2\sigma$ significance. We will hence assume that the probability of detecting a DLA is the same in the two sub-samples.

Of the 35 systems of our sample with $W_0^{\lambda 2796} \geq 0.5 \text{\AA}$ and $W_0^{\lambda 2600} \geq 0.34 \text{\AA}$, there are nine detections of HI 21cm absorption, i.e. a detection rate of $x_{21, \text{MgII}} = 26^{+12}_{-8}\%$ at a mean absorption redshift $\bar{z} = 1.1$. 34 DLAs are present amongst the 97 absorbers in the RTN06 sample that satisfy our selection criteria; this yields a detection rate of $x_{\text{DLA, MgII}} \sim 35^{+7}_{-6}\%$ for DLAs in strong MgII systems, also at a mean redshift of $\bar{z} \sim 1.1$. The implied detection rate of HI 21cm absorption in DLAs in the redshift desert is then $x_{21, \text{DLA}}(\bar{z} = 1.1) = x_{21, \text{MgII}}/x_{\text{DLA, MgII}} \sim (73 \pm 27)\%$, where we have used equation (26) of Gehrels (1986) to determine the 1σ Gaussian confidence level intervals for the ratio of two quantities governed by small-number Poisson statistics.

Fig. 5 plots the detection rate of HI 21cm absorption in DLAs as a function of redshift. While the errors are large due to the small size of each sub-sample (especially for the present MgII sample), the detection rates increase with decreasing redshift, as would be expected if the cold gas fraction in galaxies is increasing with time. The detection rate measured in the present survey is consistent with that found in low- z DLAs, suggesting that significant fractions of cold HI have already been formed in gas-rich galaxies by $z \sim 1$.

The fraction of DLAs in the redshift desert that are undetected in HI 21cm absorption is $1 - x_{21, \text{DLA}}(\bar{z} = 1.1) = (27 \pm 27)\%$; all of these non-detections must have $[T_s/f] > 800 \text{ K}$, the 3σ sensitivity limit of our survey. This implies that at least one-fourth of the DLAs in the redshift desert have high spin temperatures and/or low covering factors; this is a lower limit because some of the DLAs detected in HI 21cm absorption are also likely to have high $[T_s/f]$ ratios (see Section 5).

Fig. 6 shows the total velocity spread (FWBN) of HI 21cm absorption ΔV_{21} plotted against redshift, for the nine absorbers of this sample and the 17 DLAs with detected HI 21cm lines. Only two systems (both at $z_{\text{abs}} < 0.7$) have $\Delta V_{21} > 150 \text{ km s}^{-1}$, while $\sim 60\%$ of the absorbers in each redshift range have $\Delta V_{21} \lesssim 60 \text{ km s}^{-1}$. Overall, the velocity spread of HI 21cm absorption displays no significant evolution with redshift.

Next, no statistically-significant correlation was found in the previous section between the integrated HI 21cm optical depth

⁵ This implicitly assumes that all systems with detected HI 21cm absorption are DLAs, i.e. have $N_{\text{HI}} \geq 2 \times 10^{20} \text{ cm}^{-2}$.

EW_{21} and W_0^{12796} , W_0^{12600} , or W_0^{12852} , for the strong MgII absorbers of the full statistical sample. However, Figs. 3[A-C] show that a trend may be present between EW_{21} and the above rest equivalent widths for HI 21cm detections alone. We hence explored the possibility of a relation between EW_{21} and W_0^{12796} in high column density absorbers, considering all DLAs and HI 21cm absorbers in the literature with observations of both the HI 21cm and the MgII λ 2796 transitions. We again excluded “associated” absorbers from this analysis, as well as four DLAs with HI 21cm studies where the radio and optical sightlines are known to be different (the $z_{\text{abs}} \sim 0.437$ DLA towards 3C196, the $z_{\text{abs}} \sim 0.656$ DLA towards 3C336, and the $z_{\text{abs}} \sim 1.4$ absorbers towards QSO 0957+561A and PKS 1354+258; Briggs et al. 2001; Curran et al. 2007; Kanekar & Chengalur 2003). Fig. 7 plots EW_{21} versus W_0^{12796} for the 24 systems of this sample. The non-parametric generalized Kendall rank correlation statistic (Brown et al. 1974; Isobe et al. 1986), as implemented in the ASURV package (the BHK test), was used to test for a correlation between the two quantities, treating W_0^{12796} as the independent variable. We find the putative correlation to have $\sim 2.2\sigma$ statistical significance, with a probability of chance occurrence of $\sim 3\%$. Restricting the sample to detections of HI 21cm absorption (21 systems) increases the significance to $\sim 2.5\sigma$. This is, at most, weak evidence for a relation between the integrated HI 21cm optical depth and the rest equivalent width of the MgII λ 2796 transition.

Finally, Curran et al. (2007) suggest that the velocity spread of HI 21cm absorption and W_0^{12796} are correlated, based on a sample of 13 redshifted HI 21cm absorbers. Fig. 8 plots the total velocity spread (FWBN) of HI 21cm absorption ΔV_{21} against W_0^{12796} , for all absorbers (23 systems) with detections of both HI 21cm and MgII λ 2796 absorption (again excluding “associated” systems, but including the HI 21cm detections towards 3C196 and 3C336). No clear trend can be seen between ΔV_{21} and W_0^{12796} ; the BHK test finds the possible correlation between these quantities to have only $\sim 1.7\sigma$ significance, with a probability of chance occurrence of $\sim 11\%$. Excluding the two absorbers towards 3C196 and 3C336 does not noticeably affect the result; the correlation then has $\sim 1.6\sigma$ significance. We thus find no statistically-significant evidence for a correlation between the velocity spread of HI 21cm absorption and the rest MgII λ 2796 equivalent width.

9 THE COSMOLOGICAL MASS DENSITY OF NEUTRAL GAS

The cosmological mass density of neutral gas in DLAs, $\Omega_{\text{GAS}}(z)$, is related to their line density $n_{\text{DLA}}(z)$ (i.e. the number of DLAs per unit redshift, also sometimes referred to as the redshift number density) by the following expression (e.g. RTN06):

$$\Omega_{\text{GAS}}(z) = \frac{\mu m_{\text{H}} H_0}{c \rho_c} n_{\text{DLA}}(z) \bar{N}_{\text{HI}} \frac{E(z)}{(1+z)^2}, \quad (2)$$

where $\rho_c \equiv 3H_0^2/8\pi G$ is the critical mass density of the Universe, $\mu = 1.3$ is the correction factor for the 25% contribution of HeII to the neutral gas mass, \bar{N}_{HI} is the average HI column density of the DLAs, m_{H} is the mass of the hydrogen atom and $E(z)$ is given by

$$E(z) = [\Omega_m(1+z)^3 + (1 - \Omega_m - \Omega_\Lambda)(1+z)^2 + \Omega_\Lambda]^{1/2}. \quad (3)$$

The present survey has measured the detection rate of HI 21cm absorption in a sample of strong MgII absorbers, finding $x_{21, \text{MgII}} = 25_{-8}^{+11}\%$, at the mean absorption redshift $\bar{z} = 1.1$. The fraction of DLAs in the MgII absorber sample is then

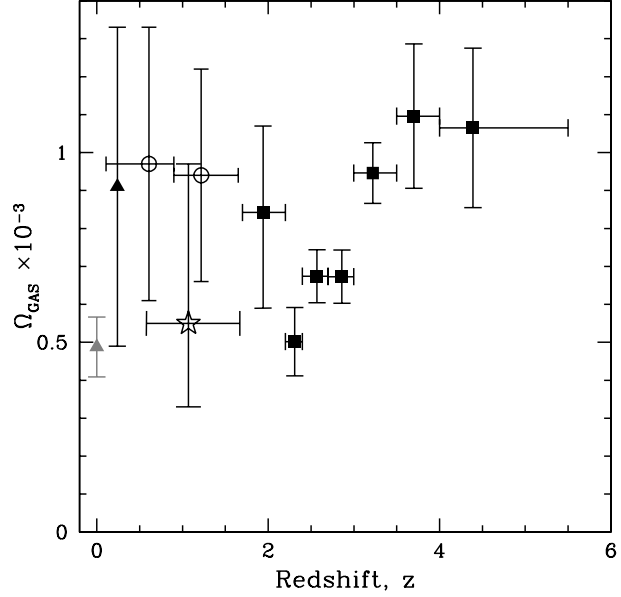


Figure 9. The cosmological mass density of neutral gas Ω_{GAS} plotted as a function of redshift, from the following techniques: (1) the HIPASS HI 21cm emission survey (grey triangle; Zwaan et al. 2005), (2) a GMRT measurement at $z \sim 0.24$, obtained by co-adding HI 21cm emission spectra of field galaxies (filled black triangle; Lah et al. 2007), (3) a survey for DLAs in strong MgII absorbers (open circles; RTN06), (4) this work (open star), and (5) traditional “blind” DLA surveys, primarily based on the SDSS-DR5 (filled squares; Prochaska & Wolfe 2008). See the main text for discussion.

$$x_{\text{DLA}, \text{MgII}}(z) = \frac{x_{21, \text{MgII}}(z)}{x_{21, \text{DLA}}(z)}, \quad (4)$$

where $x_{21, \text{DLA}}(z)$ is the detection rate of HI 21cm absorption in DLAs. In turn, the line density of DLAs is related to the above DLA fraction by the expression

$$n_{\text{DLA}}(z) = x_{\text{DLA}, \text{MgII}}(z) \times n_{\text{MgII}}(z, W_0) \quad (5)$$

where $n_{\text{MgII}}(z, W_0)$ gives the number of MgII absorbers per unit redshift with $W_0^{12796} \geq W_0$; this has been determined using large samples of strong MgII absorbers (Nestor et al. 2005). In other words, an estimate of the detection rate of HI 21cm absorption in DLAs in the redshift desert would allow us to infer Ω_{GAS} from our survey statistics [see also Lane (2000) for an estimate of the cosmological mass density of neutral hydrogen in HI 21cm absorbers, based on an HI 21cm absorption survey of MgII absorbers].

Unfortunately, we do not have an *independent* estimate of $x_{21, \text{DLA}}(z)$ in the redshift desert, due to the paucity of earlier HI 21cm absorption studies here. Note that we cannot use the value of $x_{21, \text{DLA}}(z)$ derived in Section 8 as this already includes the detection rate of HI 21cm absorption in strong MgII absorbers. However, deep searches for HI 21cm absorption (at comparable sensitivity to ours; e.g. Kanekar & Chengalur 2003) have so far been carried out in 33 “non-associated” DLAs (at $0.09 < z_{\text{abs}} < 3.4$), with 17 detections, yielding a net HI 21cm detection rate in DLAs of $x_{21, \text{DLA}}(\bar{z} = 1.7) = 52_{-12}^{+16}\%$. Assuming that $x_{21, \text{DLA}}(\bar{z} = 1.1) \approx x_{21, \text{DLA}}(\bar{z} = 1.7)$, we obtain

$$x_{\text{DLA}, \text{MgII}}(\bar{z} = 1.1) = 0.49_{-0.19}^{+0.31}. \quad (6)$$

Next, following RTN06 [see their equations (1–3)], we will use the parameterization of Nestor et al. (2005) to write

$$n_{\text{MgII}}(\bar{z}) = (1/36) \times \sum_i w_i [dn/dz]_i(\bar{z}) \quad (7)$$

where, for the i th absorber

$$[dn/dz]_i = N^* (1+z)^\alpha e^{-(W_0/W^*)(1+z)^{-\beta}}. \quad (8)$$

Here, $N^* = (1.001 \pm 0.132)$, $W^* = (0.443 \pm 0.032)\text{\AA}$, $\alpha = (0.226 \pm 0.170)$, and $\beta = (0.634 \pm 0.097)$ are constants (see the appendix of Nestor et al. 2005) and w_i is the weight given to the i th absorber, based on the fractional abundance of its class in the MgII sample of Nestor et al. (2005). All absorbers of our sample have $W_0^{12796} \geq 0.6\text{\AA}$, within the errors.⁶ 31 absorbers of our sample were selected with the additional criterion $W_0^{12600} \geq 0.5\text{\AA}$; for these systems, $w_i = 0.54$, as 54% of absorbers in the MgII sample of Nestor et al. (2005) with $W_0^{12796} \geq 0.6\text{\AA}$ also have $W_0^{12600} \geq 0.5\text{\AA}$ (RTN06). We also assume here that the fraction of strong MgII absorbers that are also strong FeII absorbers does not depend on redshift. Conversely, $w_i = 1$ for the remaining five systems, which were selected on the basis of their MgII rest equivalent width. Equation 7 then yields, for $\bar{z} = 1.1$ and $W_0 = 0.6\text{\AA}$,

$$n_{\text{MgII}}(\bar{z} = 1.1) = (0.2833 \pm 0.0065). \quad (9)$$

Replacing for $n_{\text{MgII}}(\bar{z} = 1.1)$ and $x_{\text{DLA,MgII}}(\bar{z} = 1.1)$ in equation 2 gives a DLA line redshift density of $n_{\text{DLA}}(\bar{z} = 1.1) = 0.137_{-0.054}^{+0.088}$.⁷ The only remaining unknown in equation 2 is \bar{N}_{HI} , the average HI column density in the nine HI 21cm detections of the sample. Prior to this work, all redshifted HI 21cm absorbers with observations of the Lyman- α transition have been found to be DLAs; it is thus likely that the HI 21cm absorbers detected in this survey are also DLAs. If so, it is plausible that their average HI column density is the same as that obtained by RTN06 for the DLAs detected in their MgII survey. With this assumption, $\bar{N}_{\text{HI}} = (1.07 \pm 0.23) \times 10^{21} \text{ cm}^{-2}$, where we have used the result of RTN06 from the redshift range $0.9 < z < 1.65$, where all of our HI 21cm absorbers lie. We then obtain $\Omega_{\text{GAS}}(\bar{z} = 1.1) = (0.55_{-0.22}^{+0.42}) \times 10^{-3}$.

Fig. 9 shows a comparison between estimates of the cosmological mass density of neutral gas $\Omega_{\text{GAS}}(z)$, from the following techniques (in order of increasing redshift): (1) the HIPASS survey for local HI 21cm emission (grey triangle; Zwaan et al. 2005), (2) a GMRT survey for HI 21cm emission at $z \sim 0.24$, obtained by co-adding spectra of 121 field galaxies (filled black triangle; Lah et al. 2007), (3) a survey for DLAs in strong MgII absorbers (open circles; RTN06), (4) a survey for HI 21cm absorbers in strong MgII absorbers (open star; this work), and (5) traditional “blind” DLA surveys, primarily based on the SDSS-DR3 (filled squares; Prochaska et al. 2005). The two measurements with the smallest errors, the HIPASS result at $z \sim 0$ (Zwaan et al. 2005) and the lowest-redshift SDSS-DR3 measurement at $z \sim 2.36$ (Prochaska et al. 2005), are in excellent agreement, suggesting a scenario wherein the conversion of gas to stars at $z \lesssim 2.3$ is balanced by other processes that replenish the neutral gas reservoir in galaxies. Curiously enough, however, earlier estimates of Ω_{GAS} at $0.2 < z < 2$ (from multiple techniques, the GMRT observations, the RTN06 survey and a single non-SDSS DLA measurement) are all higher than the

estimates at $z \sim 0$ and $z \sim 2.3$, although individually consistent with these measurements due to their far larger errors. While the estimate from the present survey, $\Omega_{\text{GAS}}(\bar{z} = 1.1) = (0.55_{-0.22}^{+0.42}) \times 10^{-3}$ is in good agreement with the two high-sensitivity results, the error bars on our result are also large and we cannot rule out the values obtained by Rao et al. (2006).

We emphasize that the present result for Ω_{GAS} assumes that the average HI column density of our HI 21cm absorbers is the same as that in the DLA sample of RTN06. Direct measurements of the HI column density of these absorbers through spectroscopy in the Lyman- α line would allow a measurement of \bar{N}_{HI} for the sample, obviating the need for this assumption. Equally important, we have assumed $x_{21,\text{DLA}}(\bar{z} = 1.1) \approx x_{21,\text{DLA}}(\bar{z} = 1.7)$. As seen in Section 8, the detection rate of HI 21cm absorption in DLAs appears to increase with decreasing redshift, implying that $x_{21,\text{DLA}}(\bar{z} = 1.1)$ is likely to be higher than $x_{21,\text{DLA}}(\bar{z} = 1.7)$. In fact, the estimated average value $x_{21,\text{DLA}}(\bar{z} = 1.7) = (52_{-12}^{+16})\%$ from the DLA sample is lower than the value $x_{21,\text{DLA}}(\bar{z} = 1.1) = (73 \pm 27)\%$ obtained in Section 8. In other words, this assumption could result in an *upward* bias in our estimate of Ω_{GAS} .

Unlike direct surveys for DLAs in MgII absorber samples (e.g. Rao & Turnshek 2000; RTN06), observing time on space-based facilities is only needed for the last stage of the present survey, the measurements of the HI column density for detections of HI 21cm absorption. Deep HI 21cm absorption surveys of large samples of MgII-selected absorbers towards radio-loud quasars thus provide an interesting avenue to find new samples of DLAs, and determine Ω_{GAS} , at $z < 1.7$, with relatively little expenditure of observing time on space telescopes.

10 SUMMARY

We report results from a search for HI 21cm absorption in 55 strong MgII absorbers at $0.58 \lesssim z_{\text{abs}} \lesssim 1.70$ towards radio-loud quasars, with $W_0^{12796} \geq 0.5\text{\AA}$. The survey yielded nine detections of HI 21cm absorption (one of which is still tentative), all at $1.17 < z_{\text{abs}} < 1.68$, and 27 strong constraints on the HI 21cm optical depth ($\tau_{3\sigma} \lesssim 0.013$, per $\sim 10 \text{ km s}^{-1}$). Six other systems had weaker constraints on the HI 21cm optical depth ($\tau_{3\sigma} \sim 0.02 - 0.06$, per $\sim 10 \text{ km s}^{-1}$), while data on 13 targets were affected by RFI and were hence not useful.

HI column density estimates are available in the literature for a few of the MgII absorbers of our sample, two of which, at $z \sim 0.9115$ towards 2149+212 and $z \sim 1.4106$ towards 2003–025, are known damped Lyman- α systems. Our detection of HI 21cm absorption towards 2003–025 yields an absorber spin temperature of $T_s = (905 \pm 380) \times f \text{ K}$, while the non-detection towards 2149+212 gives the 3σ limit $T_s > 2700 \times f \text{ K}$.

Including three systems from the literature and excluding all “associated” absorbers, our statistical sample of strong MgII absorbers consists of 36 systems at $0.58 < z_{\text{abs}} < 1.68$, with $W_0^{12796} \geq 0.57\text{\AA}$, and with either detections of HI 21cm absorption or, for non-detections, $\tau_{21} \lesssim 0.013$ per $\sim 10 \text{ km s}^{-1}$. This implies a detection rate of $x_{21,\text{MgII}}(\bar{z} = 1.1) = 25_{-8}^{+11}\%$ for HI 21cm absorption in strong MgII absorbers. Comparing the detection rates of HI 21cm absorption and DLAs in similarly-selected samples of strong MgII absorbers, we estimate that the detection rate of HI 21cm absorption in DLAs in the redshift desert is $x_{21}(\bar{z} = 1.1) \sim (73 \pm 27)\%$. This lies between the estimates of detection rates at lower and higher redshifts, $x_{21}(\bar{z} \sim 0.4) \sim 85_{-28}^{+15}\%$ and $x_{21}(\bar{z} \sim 2.7) \sim 33_{-13}^{+20}\%$, although all three estimates have large errors. If the relatively-high

⁶ Note that one of our absorbers has $W_0^{12796} = 0.57\text{\AA}$, although consistent with 0.6\AA within the errors. We estimate that using a threshold width of $W_0^{12796} = 0.57\text{\AA}$ in equation 8 would change our results by $< 5\%$, much below our actual errors. We hence choose to retain a threshold width of $W_0^{12796} = 0.6\text{\AA}$, for which the fraction of systems with $W_0^{12600} \geq 0.5\text{\AA}$ is quoted by RTN06.

⁷ For all cases of error propagation with asymmetric errors, we used 10^5 Monte-Carlo runs to derive the 1σ confidence intervals on the final quantity.

detection rate of H I 21cm absorption in DLAs in the redshift desert is confirmed in larger samples, it would imply that significant fractions of cold H I are present in normal galaxies by $z \sim 1$. The $\sim (27 \pm 27)\%$ of DLAs that are not detected in H I 21cm absorption must have $[T_s/f] > 800$ K, implying that at least one-fourth of the DLAs in the redshift desert have high spin temperatures and/or low covering factors.

Contrary to earlier results based on smaller samples, we find no statistically-significant evidence for a correlation between the total velocity spread of H I 21cm absorption and the rest MgII $\lambda 2796$ equivalent width in DLAs and strong MgII absorbers. We find a weak (2.2σ) correlation between the integrated H I 21cm optical depth and W_0^{12796} , for a sample consisting of DLAs and H I 21cm detections alone.

We have used the net H I 21cm detection rate in strong MgII absorbers to estimate the cosmological mass density in neutral gas in DLAs, obtaining $\Omega_{\text{GAS}}(\bar{z} = 1.1) = (0.55^{+0.42}_{-0.22}) \times 10^{-3}$. This assumes that (1) the average H I column density of the H I 21cm absorbers is the same as that in the DLA sample of RTN06, and (2) the detection rate of H I 21cm absorption in DLAs at $z \sim 1.1$ is the same as that at $z \sim 1.7$. While this estimate has large errors, it is in good agreement with estimates of Ω_{GAS} in both the local universe and at $z \sim 2.2$, and somewhat lower than earlier estimates in the redshift desert from MgII absorber samples. Future deep searches for H I 21cm absorption in large samples of strong MgII absorbers should allow more accurate estimates of Ω_{GAS} in the redshift desert, without significant requirements of observing time on space telescopes.

For the nine detections of H I 21cm absorption, spectroscopy in the Lyman- α line to measure their H I column densities, and low-frequency VLBI continuum observations of the background QSOs to determine the absorber covering factors, will allow estimates of the absorber spin temperatures. For systems with narrow H I 21cm profiles (e.g. 2337–011, 2355–106 and 0105–008), high-resolution optical spectroscopy in the low-ionization metal lines will allow a probe of evolution in the fundamental constants. These observations are now in progress.

11 ACKNOWLEDGMENTS

We thank Carl Bignell, Bob Garwood, Toney Minter, Frank Ghigo and Glen Langston for much help with the GBT observations and data analysis, and Ishwara-Chandra and Nimisha Kantharia for help with the scheduling of the GMRT observations. We thank the staff of the GMRT who made these observations possible; the GMRT is run by the National Centre for Radio Astrophysics of the Tata Institute of Fundamental Research. The National Radio Astronomy Observatory is operated by Associated Universities, Inc, under co-operative agreement with the National Science Foundation. This research has made use of the NASA/IPAC Extragalactic Database (NED) which is operated by the Jet Propulsion Laboratory, California Institute of Technology, under contract with the National Aeronautics and Space Administration. This research has also made use of the SAO/NASA Astrophysics Data System. NK acknowledges support from the Max-Planck Foundation and an NRAO Jansky Fellowship. We also thank an anonymous referee for useful comments on an earlier draft of this manuscript.

REFERENCES

- Akerman C. J., Ellison S. L., Pettini M., Steidel C. C., 2005, *A&A*, 440, 499
- Aldcroft T. L., Bechtold J., Elvis M., 1994, *ApJS*, 93, 1
- Barthel P. D., Tytler D. R., Thomson B., 1990, *A&AS*, 82, 339
- Beasley A. J., Gordon D., Peck A. B., Petrov L., MacMillan D. S., Fomalont E. B., Ma C., 2002, *ApJS*, 141, 13
- Becker R. H., White R. L., Helfand D. J., 1995, *ApJ*, 450, 559
- Braun R., Walterbos R., 1992, *ApJ*, 386, 120
- Briggs F. H., de Bruyn A. G., Vermeulen R. C., 2001, *A&A*, 373, 113
- Briggs F. H., Wolfe A. M., 1983, *ApJ*, 268, 76
- Briggs F. H., Wolfe A. M., Liszt H. S., Davis M. M., Turner K. L., 1989, *ApJ*, 341, 650
- Brown B. W. M., Hollander M., Korwar R. M., 1974, in Proschan F., Serfling R. J., eds, *Reliability and Biometry Philadelphia: SIAM*, p. 327
- Brown R. L., Mitchell K. J., 1983, *ApJ*, 264, 87
- Brown R. L., Roberts M. S., 1973, *ApJ*, 184, L7
- Brown R. L., Spencer R. E., 1979, *ApJ*, 230, L1
- Carilli C. L., Lane W. M., de Bruyn A. G., Braun R., Miley G. K., 1996, *AJ*, 111, 1830
- Chen H.-W., Lanzetta K. M., 2003, *ApJ*, 597, 706
- Chengalur J. N., Kanekar N., 1999, *MNRAS*, 302, L29
- Chengalur J. N., Kanekar N., 2000, *MNRAS*, 318, 303
- Condon J. J., Cotton W. D., Greisen E. W., Yin Q. F., Perley R. A., Taylor G. B., Broderick J. J., 1998, *AJ*, 115, 1693
- Curran S. J., Murphy M. T., Pihlström Y. M., Webb J. K., Purcell C. R., 2005, *MNRAS*, 356, 1509
- Curran S. J., Tzanavaris P., Murphy M. T., Webb J. K., Pihlström Y. M., 2007, *MNRAS*, 381, L6
- Curran S. J., Tzanavaris P., Pihlström Y. M., Webb J. K., 2007, *MNRAS*, 382, 1331
- Dessauges-Zavadsky M., Calura F., Prochaska J. X., D’Odorico S., Matteucci F., 2007, *A&A*, 470, 431
- Douglas J. N., Bash F. N., Bozayan F. A., Torrence G. W., Wolfe C., 1996, *AJ*, 111, 1945
- Ellison S. L., Churchill C. W., Rix S. A., Pettini M., 2004, *ApJ*, 615, 118
- Ellison S. L., Yan L., Hook I. M., Pettini M., Wall J. V., Shaver P., 2001, *A&A*, 379, 393
- Ellison S. L., York B. A., Pettini M., Kanekar N., 2008, *MNRAS*, 388, 1349
- Fomalont E. B., Frey S., Paragi Z., Gurvits L. I., Scott W. K., Taylor A. R., Edwards P. G., Hirabayashi H., 2000, *ApJS*, 131, 95
- Gehrels N., 1986, *ApJ*, 303, 336
- Gupta N., Srianand R., Petitjean P., Khare P., Saikia D. J., York D. G., 2007, *ApJ*, 654, L111
- Hodges M. W., Mutel R. L., Phillips R. B., 1984, *AJ*, 89, 1327
- Hopkins A. M., 2004, *ApJ*, 615, 209
- Isobe T., Feigelson E. D., Nelson P. I., 1986, *ApJ*, 306, 490
- Jackson C. A., Wall J. V., Shaver P. A., Kellermann K. I., Hook I. M., Hawkins M. R. S., 2002, *A&A*, 386, 97
- Jorgenson R. A., Wolfe A. M., Prochaska J. X., Lu L., Howk J. C., Cooke J., Gawiser E., Gelino D. M., 2006, *ApJ*, 646, 730
- Kanekar N., 2008, *Mod. Phys. Lett. A*, 23, 2711
- Kanekar N., Briggs F. H., 2004, *New Astr. Rev.*, 48, 1259
- Kanekar N., Chengalur J. N., 2001, *A&A*, 369, 42
- Kanekar N., Chengalur J. N., 2003, *A&A*, 399, 857
- Kanekar N., Chengalur J. N., Lane W. M., 2007, *MNRAS*, 375,

- 1528
- Kanekar N., Lane W. M., Momjian E., Briggs F. H., Chengalur J. N., 2009, *MNRAS*, 394, L61
- Kanekar N., Subrahmanyan R., Ellison S. L., Lane W. M., Chengalur J. N., 2006, *MNRAS*, 370, L46
- Khare P., Kulkarni V. P., Lauroesch J. T., York D. G., Crotts A. P. S., Nakamura O., 2004, *ApJ*, 616, 86
- Kulkarni V. P., Fall S. M., 2002, *ApJ*, 580, 732
- Kulkarni V. P., Fall S. M., Lauroesch J. T., York D. G., Welty D. E., Khare P., Truran J. W., 2005, *ApJ*, 618, 68
- Kunert M., Marecki A., Spencer R. E., Kus A. J., Niezgoda J., 2002, *A&A*, 391, 47
- Lah P., Chengalur J. N., Briggs F. H., Colless M., de Propriis R., Pracy M. B., de Blok W. J. G., Fujita S. S., Ajiki M., Shioya Y., Nagao T., Murayama T., Taniguchi Y., Yagi M., Okamura S., 2007, *MNRAS*, 376, 1357
- Lane W., Smette A., Briggs F., Rao S., Turnshek D., Meylan G., 1998, *AJ*, 116, 26
- Lane W. M., 2000, Ph.D. thesis. University of Groningen
- Lane W. M., Briggs F. H., 2001, *ApJ*, 561, L27
- le Brun V., Bergeron J., Boissé P., Deharveng J.-M., 1997, *A&A*, 321, 733
- Liszt H., 2001, *A&A*, 371, 698
- Madau P., Ferguson H. C., Dickinson M. E., Giavalisco M., Steidel C. C., Fruchter A., 1996, *MNRAS*, 283, 1388
- Meiring J. D., Kulkarni V. P., Khare P., Bechtold J., York D. G., Cui J., Lauroesch J. T., Crotts A. P. S., Nakamura O., 2006, *MNRAS*, 370, 43
- Nestor D. B., Turnshek D. A., Rao S. M., 2005, *ApJ*, 628, 637
- Pei Y. C., Fall M., Hauser M. G., 1999, *ApJ*, 522, 604
- Peterson B. M., Foltz C. B., 1980, *ApJ*, 242, 879
- Peterson B. M., Strittmatter P. A., 1978, *ApJ*, 226, 21
- Pettini M., Ellison S. L., Steidel C. C., Bowen D. V., 1999, *ApJ*, 510, 576
- Prochaska J. X., Gawiser E., Wolfe A. M., Castro S., Djorgovski S. G., 2003, *ApJ*, 595, L9
- Prochaska J. X., Herbert-Fort S., 2004, *PASP*, 116, 622
- Prochaska J. X., Herbert-Fort S., Wolfe A. M., 2005, *ApJ*, 635, 123
- Prochaska J. X., Wolfe A. M., 1997, *ApJ*, 487, 73
- Prochaska J. X., Wolfe A. M., 2008, *arXiv/0811.2003*
- Prochaska J. X., Wolfe A. M., Howk J. C., Gawiser E., Burles S. M., Cooke J., 2007, *ApJS*, 171, 29
- Prochter G. E., Prochaska J. X., Burles S. M., 2006, *ApJ*, 639, 766
- Rao S. M., Nestor D. B., Turnshek D. A., Lane W. M., Monier E. M., Bergeron J., 2003, *ApJ*, 595, 94
- Rao S. M., Turnshek D. A., 2000, *ApJS*, 130, 1
- Rao S. M., Turnshek D. A., Nestor D. B., 2006, *ApJ*, 636, 610
- Rengelink R. B., Tang Y., de Bruyn A. G., Miley G. K., Bremer M. N., Röttgering H. J. A., Bremer M. A. R., 1997, *A&AS*, 124, 259
- Roberts M. S., Brown R. L., Brundage W. D., Rots A. H., Haynes M. P., Wolfe A. M., 1976, *AJ*, 81, 293
- Rohlf K., Wilson T. L., 2006, *Tools of Radio Astronomy*. Berlin: Springer
- Sargent W. L. W., Steidel C. C., Boksenberg A., 1988, *ApJ*, 334, 22
- Sargent W. L. W., Steidel C. C., Boksenberg A., 1989, *ApJS*, 69, 703
- Srianand R., Gupta N., Petitjean P., 2007, *MNRAS*, 375, 584
- Srianand R., Gupta N., Petitjean P., Noterdaeme P., Saikia D. J., 2008, *MNRAS*, 391, L69
- Steidel C. C., Sargent W. L. W., 1992, *ApJS*, 80, 1
- Wild V., Hewett P. C., 2005, *MNRAS*, 361, L30
- Wolfe A. M., Briggs F. H., Jauncey D. L., 1981, *ApJ*, 248, 460
- Wolfe A. M., Briggs F. H., Turnshek D. A., Davis M. M., Smith H. E., Cohen R. D., 1985, *ApJ*, 294, L67
- Wolfe A. M., Broderick J. J., Condon J. J., Johnston K. J., 1976, *ApJ*, 208, L47
- Wolfe A. M., Davis M. M., 1979, *AJ*, 84, 699
- Wolfe A. M., Gawiser E., Prochaska J. X., 2003, *ApJ*, 593, 235
- Wolfe A. M., Gawiser E., Prochaska J. X., 2005, *ARA&A*, 43, 861
- Wolfe A. M., Turnshek D. A., Smith H. E., Cohen R. D., 1986, *ApJS*, 61, 249
- York B. A., Kanekar N., Ellison S. L., Pettini M., 2007, *MNRAS*, 382, L53
- Young L. M., Lo K. Y., 1997, *ApJ*, 490, 710
- Zwaan M. A., Meyer M. J., Staveley-Smith L., Webster R. L., 2005, *MNRAS*, 359, L30
- Zwaan M. A., van der Hulst J. M., Briggs F. H., Verheijen M. A. W., Ryan-Weber E. V., 2005, *MNRAS*, 364, 1467